J. Comput. Phys. 495 (2023) 112562

Contents lists available at ScienceDirect

Journal of Computational Physics

journal homepage: www.elsevier.com/locate/jcp

Efficient interior penalty discontinuous Galerkin projection method with unconditional energy stability and second-order temporal accuracy for the incompressible magneto-hydrodynamic system

Guang-an Zou [a], Bo Wang [b], Xiaofeng Yang [c,*]

[a] School of Mathematics and Statistics; Henan Engineering Research Center for Artificial Intelligence Theory and Algorithms; Henan University, Kaifeng 475004, PR China

[b] School of Mathematics and Statistics; Henan Engineering Research Center for Artificial Intelligence Theory and Algorithms; Henan Key Laboratory of Earth System Observation and Modeling, Henan University, Kaifeng 475004, PR China

[c] Department of Mathematics, University of South Carolina, Columbia, SC 29208, USA

ARTICLE INFO

Keywords:
Magneto-hydrodynamic equations
Fully-decoupled
Rotational pressure-correction
DG method
Numerical examples

ABSTRACT

In this paper, we propose a novel interior penalty discontinuous Galerkin projection method for the incompressible magneto-hydrodynamic equations. The scheme is employed by an implicit-explicit treatment of the nonlinear coupling terms and a second-order rotational pressure-correction scheme for dealing with the Navier-Stokes equations. One noteworthy aspect of this scheme is the introduction of an additional stabilization term to Maxwell's equations, which allows for the explicit treatment of the coupled nonlinear terms and the decoupling of computations for the magnetic and velocity fields, ultimately leading to the achievement of desired linearity, full decoupling, second-order accuracy in time, and unconditional energy stability. The obtained scheme is easy to implement because one only needs to solve a few decoupled linear equations at each time step. We rigorously prove the unique solvability and unconditional energy stability of the developed scheme and present a series of numerical examples to demonstrate the accuracy, stability, and efficiency of the proposed scheme.

1. Introduction

The magneto-hydrodynamic (MHD) system, a mathematical model that combines the Navier-Stokes equations, describing fluid mechanics, with Maxwell's equations, which deal with electromagnetism, has emerged as an indispensable tool for investigating the complex hydrodynamic behaviors of conducting fluids. Its diverse applications span scientific and engineering fields, including but not limited to plasma confinement, liquid-metal cooling of nuclear reactors, and magnetic drug targeting, as demonstrated in [19,25,43]. Due to its potential for widespread applications, numerous numerical methods have been developed for solving the MHD system and have garnered significant attention from researchers and engineers in recent years, where some notable works on this topic can be found in [1,6,11,15,24,31,45], among others cited therein.

* Corresponding author.
E-mail addresses: zouguangan@henu.edu.cn (G.-a. Zou), wb2008@henu.edu.cn (B. Wang), xfyang@math.sc.edu (X. Yang).

https://doi.org/10.1016/j.jcp.2023.112562
Received 5 May 2023; Received in revised form 1 October 2023; Accepted 11 October 2023

Available online 16 October 2023
0021-9991/

Designing effective numerical algorithms for MHD systems poses a formidable challenge due to the nonlinear coupling between the velocity and magnetic fields, which arises from the advection and Lorentz forces. In particular, requirements such as ensuring that the proposed scheme is both linear and fully decoupled, while simultaneously preserving the law of energy dissipation in discrete systems, can make the development of numerical schemes extremely complex. A "linear" numerical scheme is one in which only a few linear subsystems need to be solved at each time step without nonlinear iterations, while a "fully decoupled" approach is one in which each unknown variable can be solved independently at least at each time step without being stirred up with other unknowns. Being able to achieve both linearity and full decoupling with energy stability is a challenging task, since most existing schemes tend to sacrifice one property in favor of the other. Therefore, designing an efficient energy-stable numerical algorithm to satisfy both requirements remains an active research area in the numerical computation of MHD systems.

We review much of the current work that has been done, including recent attempts, to create linear and decoupled algorithms for simulating the MHD system. The authors in [55] presented a numerical scheme for a two-dimensional MHD system in a decoupled manner. However, the scheme exhibits only conditional energy stability, which imposes a constraint on the maximum permissible time-step. In [51,58] the authors proposed an unconditional energy stable scheme, however, it is only partially decoupled, and cannot achieve complete decoupling. In [3,4], the authors presented a first-order pressure-projection scheme for solving the MHD system, however, it should be noted that this scheme maintains coupling between the velocity field and magnetic field. In [38], the authors proposed a second-order BDF finite element scheme for the hybrid MHD system, however, the scheme doesn't ensure any discrete energy stability. In [50], the authors developed a Crank-Nicolson type finite element method for the MHD system. However, it should be noted that this scheme is only partially decoupled. In [54,56], a linear scheme with unconditional energy stability is developed where the full decoupling is achieved by introducing an auxiliary intermediate velocity variable, however, the scheme is only first-order accurate in time. A recent work presented in [57] developed the first linear and fully decoupled scheme that achieves second-order accuracy and unconditional energy stability, utilizing the "zero-energy-contribution" method. Although the algorithm presented in [57] is notably effective, the numerical method developed in this paper surpasses it in three aspects. First, the scheme proposed in this paper is more computationally efficient since each equation is solved independently, without the need of doubling the computational effort by splitting it into two equations, whereas in [57], each equation needs to be split into two. Second, it requires no artificial pressure boundary conditions to decouple the pressure and velocity for solving the Navier-Stokes equations. Third, the numerical scheme given in [57] uses the conforming finite element method (FEM) for spatial discretization. In contrast, the numerical scheme proposed in this paper uses the discontinuous Galerkin FEM method, which makes use of discontinuous piecewise polynomials as trial and test functions. The discontinuous Galerkin (DG) method has several more attractive features, including local conservation, high order accuracy, adaptability, and ease of implementation, as evidenced by [12,13,41,46,60,62], when compared to the continuous FEM. Moreover, most existing FEM used conforming elements to approximate the MHD system, resulting in a lack of local conservation for both magnetic field and velocity field, as highlighted in [45].

It is noteworthy that some previous studies have also utilized DG methods to solve MHD systems. However, these studies usually focused on stable MHD equations bypassing the time derivative problem, or on fully coupled and/or nonlinear schemes. For example, in [35,45], the authors proposed DG methods for the MHD system, but only steady MHD equations are considered and the obtained scheme is fully-coupled. In [53], the DG method was used for the viscous MHD equations, however, the scheme is nonlinear and fully coupled. In [39], the authors investigated a locally divergence-free DG scheme for the ideal MHD equations, but the magnetic field and velocity field are still coupled together. In [8], the authors proposed a DG method for a reduced resistive MHD system in 2D, but the scheme is highly nonlinear and coupled too. Hence, as far as the authors are aware, no DG methods for MHD systems have been identified to possess the desirable properties of full decoupling, linearity, unconditional energy stability and second-order temporal accuracy, which is the goal of this paper.

To achieve the objective of obtaining a numerical scheme with the above-mentioned desirable characteristics for the MHD system, we employ several approaches in combination. First, we introduce an artificial stabilization term into Maxwell's equations to decouple the magnetic field from the velocity field and maintain second-order temporal accuracy. This stabilization term addresses the stability issue that arises from the explicit treatment of the coupled nonlinear term, and it can also be considered as a second-order perturbation to the magnetic equation at the discrete level. Second, we adopt a second-order rotational pressure-correction scheme for solving the Navier-Stokes equations, which offers the advantage of decoupling the computations of the pressure and velocity, and eliminates the need for artificial pressure boundary conditions. Third, we make use of the DG method to discretize the spatial domain, resulting in a fully discrete scheme. The combination of these approaches enables us to obtain an effective and easy-to-implement numerical scheme that satisfies all the desired characteristics, namely, full decoupling, linearity, second-order accuracy in time, and unconditional energy stability. In addition, we conduct extensive numerical experiments to verify the stability and accuracy of the proposed scheme, which included benchmark simulations of the Kelvin-Helmholtz (K-H) instability, MHD rotator, and Taylor-Green vortex.

The outline of this paper is as follows. In Section 2, we present the time-dependent MHD system and derive its energy dissipation law in terms of the underlying partial differential equations (PDEs). In Section 3, we construct the fully discrete DG scheme for solving the MHD system which is a novel linear scheme with second-order time accuracy and fully-decoupled structure, and present the scheme's unique solvability and unconditional energy stability. Section 4 presents the results of numerical simulations that demonstrate the accuracy and efficiency of our proposed scheme. Finally, some concluding remarks are presented in Section 5.

2. The MHD system

We consider numerical approximations of the incompressible MHD system, which is comprised of the Maxwell equations coupled with the incompressible Navier-Stokes equations (see [23,54,56]), and reads as:

$$\boldsymbol{m}_t + \nu_m \nabla \times (\nabla \times \boldsymbol{m}) - \nabla \times (\boldsymbol{u} \times \boldsymbol{m}) = 0, \tag{2.1a}$$

$$\boldsymbol{u}_t + \boldsymbol{u} \cdot \nabla \boldsymbol{u} - \nu \Delta \boldsymbol{u} + \nabla p + \kappa \boldsymbol{m} \times \nabla \times \boldsymbol{m} = 0, \tag{2.1b}$$

$$\nabla \cdot \boldsymbol{u} = 0, \tag{2.1c}$$

$$\nabla \cdot \boldsymbol{m} = 0, \tag{2.1d}$$

where $(\boldsymbol{x}, t) \in \Omega \times [0, T]$ with $\Omega \subset \mathbb{R}^d, d = 2, 3$. The unknown variables in (2.1) are the magnetic field $\boldsymbol{m}$, velocity field $\boldsymbol{u}$, and pressure p. Regarding the physical parameters that describe the fluid, $R_e = \nu^{-1}$ is the Reynolds number, $R_m = \nu_m^{-1}$ denotes the magnetic Reynolds number, and κ stands for the coupling parameter, respectively. We consider the following boundary conditions:

$$\boldsymbol{n} \times \boldsymbol{m} = 0, \ \boldsymbol{u} = 0 \text{ on } \partial\Omega, \tag{2.2}$$

and the following initial conditions:

$$\boldsymbol{m}(\boldsymbol{x}, 0) = \boldsymbol{m}_0, \ \boldsymbol{u}(\boldsymbol{x}, 0) = \boldsymbol{u}_0 \text{ in } \Omega, \tag{2.3}$$

with $\nabla \cdot \boldsymbol{m}_0 = 0, \nabla \cdot \boldsymbol{u}_0 = 0$, where $\boldsymbol{n}$ denotes the unit outward normal vector on $\partial\Omega$.

We first fix some notations here. For $1 \le p \le \infty, 0 \le s \le \infty$, denoted by $L^p(\Omega)$ and $W^{s,p}(\Omega)$ the usual Lebesgue and Sobolev spaces, with the norms $\|\cdot\|_{L^p}$ and $\|\cdot\|_{W^{s,p}}$, respectively. The inner product and norm of $L^2(\Omega)$ are represented by $(\cdot,\cdot)$ and $\|\cdot\|$, respectively. Additionally, we define several spaces as follows:

$$\boldsymbol{X} = \boldsymbol{H}_0^1(\Omega) = \{\boldsymbol{v} \in [H^1(\Omega)]^d : \boldsymbol{v} = 0 \text{ on } \partial\Omega\},$$

$$\boldsymbol{H}(curl, \Omega) = \{\boldsymbol{w} \in [L^2(\Omega)]^d : \nabla \times \boldsymbol{w} \in [L^2(\Omega)]^d\},$$

$$M = L_0^2(\Omega) = \{q \in L^2(\Omega) : \int_\Omega q \, dx = 0\},$$

$$\boldsymbol{Y} = \boldsymbol{H}_0(curl; \Omega) = \{\boldsymbol{w} \in \boldsymbol{H}(curl, \Omega) : \boldsymbol{n} \times \boldsymbol{w} = 0 \text{ on } \partial\Omega\}.$$

Using the above notations, the weak formulation of the MHD system (2.1)-(2.3) reads as follows. Find $(\boldsymbol{m}, \boldsymbol{u}, p) \in \boldsymbol{Y} \times \boldsymbol{X} \times M$ such that for all $(\boldsymbol{w}, \boldsymbol{v}, q) \in \boldsymbol{Y} \times \boldsymbol{X} \times M$,

$$(\boldsymbol{m}_t, \boldsymbol{w}) + \nu_m(\nabla \times \boldsymbol{m}, \nabla \times \boldsymbol{w}) + \nu_m(\nabla \cdot \boldsymbol{m}, \nabla \cdot \boldsymbol{w}) - (\boldsymbol{u} \times \boldsymbol{m}, \nabla \times \boldsymbol{w}) = 0, \tag{2.4a}$$

$$(\boldsymbol{u}_t, \boldsymbol{v}) + \nu(\nabla \boldsymbol{u}, \nabla \boldsymbol{v}) + b(\boldsymbol{u}, \boldsymbol{u}, \boldsymbol{v}) - (p, \nabla \cdot \boldsymbol{v}) + \kappa(\boldsymbol{m} \times \nabla \times \boldsymbol{m}, \boldsymbol{v}) = 0, \tag{2.4b}$$

$$(\nabla \cdot \boldsymbol{u}, q) = 0, \tag{2.4c}$$

where the trilinear form $b(\cdot,\cdot,\cdot)$ is given by

$$b(\boldsymbol{u}, \boldsymbol{v}, \boldsymbol{w}) = \frac{1}{2} \int_\Omega (\boldsymbol{u} \cdot \nabla)\boldsymbol{v} \cdot \boldsymbol{w} d\boldsymbol{x} - \frac{1}{2} \int_\Omega (\boldsymbol{u} \cdot \nabla)\boldsymbol{w} \cdot \boldsymbol{v} d\boldsymbol{x}, \ \forall \boldsymbol{u}, \boldsymbol{v}, \boldsymbol{w} \in \boldsymbol{X}.$$

It is easy to verify that the trilinear form b satisfies

$$b(\boldsymbol{u}, \boldsymbol{v}, \boldsymbol{v}) = 0. \tag{2.5}$$

Remark 2.1. Note that the additional term $\nu_m(\nabla \cdot \boldsymbol{m}, \nabla \cdot \boldsymbol{w})$ added in (2.4a) was proposed by the work in [5,14,24,31,32,59], which can be understood as an exact penalty formulation for explicitly enforcing the divergence-free constraint on the magnetic field. By using this approach and dropping the divergence-free condition of $\boldsymbol{m}$, the numerical approximation process is simplified, and a one-graph implementation and arbitrary-order Lagrangian interpolations for the magnetic field are allowed. Additionally, this method does not require precise calculations of three-dimensional singular functions in the 3D case.

The energy law can be shown to hold for the system (2.4), as stated in the following lemma.

Lemma 2.2. *Assuming that $(\boldsymbol{m}, \boldsymbol{u}, p)$ is solution of the weak form of the MHD system (2.4), then the following energy law holds*

$$\frac{d}{dt}\mathbb{E}(\boldsymbol{m}, \boldsymbol{u}) = -\nu\|\nabla \boldsymbol{u}\|^2 - \kappa\nu_m\|\nabla \times \boldsymbol{m}\|^2 - \kappa\nu_m\|\nabla \cdot \boldsymbol{m}\|^2 \le 0, \tag{2.6}$$

where the total energy $\mathbb{E}(\boldsymbol{m}, \boldsymbol{u})$ is defined as

$$\mathbb{E}(\boldsymbol{m},\boldsymbol{u}) = \frac{\kappa}{2}\|\boldsymbol{m}\|^2 + \frac{1}{2}\|\boldsymbol{u}\|^2.$$

Proof. By taking $\boldsymbol{w} = \kappa\boldsymbol{m}$ in (2.4a), $\boldsymbol{v} = \boldsymbol{u}$ in (2.4b) and $q = p$ in (2.4c), and using (2.5), we get

$$\kappa(\boldsymbol{m}_t,\boldsymbol{m}) + \kappa\nu_m\|\nabla\times\boldsymbol{m}\|^2 + \kappa\nu_m\|\nabla\cdot\boldsymbol{m}\|^2 - \kappa(\boldsymbol{u}\times\boldsymbol{m},\nabla\times\boldsymbol{m}) = 0, \tag{2.7}$$

and

$$(\boldsymbol{u}_t,\boldsymbol{u}) + \nu\|\nabla\boldsymbol{u}\|^2 + \kappa(\boldsymbol{m}\times\nabla\times\boldsymbol{m},\boldsymbol{u}) = 0. \tag{2.8}$$

By taking the summation of (2.7) and (2.8), we obtain

$$\frac{\kappa}{2}\frac{d}{dt}\|\boldsymbol{m}\|^2 + \frac{1}{2}\frac{d}{dt}\|\boldsymbol{u}\|^2 + \nu\|\nabla\boldsymbol{u}\|^2 + \kappa\nu_m\|\nabla\times\boldsymbol{m}\|^2 + \kappa\nu_m\|\nabla\cdot\boldsymbol{m}\|^2 = 0, \tag{2.9}$$

where we use the following identity

$$(\boldsymbol{u}\times\boldsymbol{m},\nabla\times\boldsymbol{m}) = (\boldsymbol{m}\times\nabla\times\boldsymbol{m},\boldsymbol{u}). \tag{2.10}$$

Therefore, the desired result (2.6) follows from (2.9) directly, which indicates that the total free energy decays. □

3. Fully discrete DG scheme

In this section, we will design a novel fully-discrete scheme with unconditional energy stability and second-order temporal accuracy for solving the MHD system (2.1)-(2.3), where we achieve space discretization using the DG method, while time discretization is accomplished using the backward difference formula of second order (BDF2). Furthermore, we rigorously demonstrate the well-posedness and energy stability of the proposed method.

3.1. Numerical scheme

Let $\tau > 0$ be the time step size and set $t_k = k\tau$ for $0 \le k \le N = [T/\tau]$, where $T > 0$ is the final time. For a smooth function $\boldsymbol{v}$, the approximation of $\boldsymbol{v}$ at time t_k is denoted as $\boldsymbol{v}^k = \boldsymbol{v}(t_k)$. To simplify the presentation, we introduce the following notations

$$\hat{\boldsymbol{u}}^* = 2\boldsymbol{u}^k - \boldsymbol{u}^{k-1},\ \hat{\boldsymbol{m}}^* = 2\boldsymbol{m}^k - \boldsymbol{m}^{k-1},$$

for $k = 1, 2, \cdots, N$.

We consider a quasi-uniform partition $\mathcal{E}_h$ of Ω consisting of the elements E, where E denotes a triangle in $\mathbb{R}^2$ or tetrahedrons in $\mathbb{R}^3$. We define $\mathcal{F}_h = \mathcal{F}_h^I \cup \mathcal{F}_h^B$, denoted by $\mathcal{F}_h^I$ the set of all interior faces of $\mathcal{E}_h$, and by $\mathcal{F}_h^B$ the set of all boundary faces. Let h_E denote the diameter of mesh elements E, and h_e is the diameter of the face e, denoted by h the maximum element diameter. Let $\boldsymbol{n}_E$ be the unit outward normal vector on ∂E, and let $e = \partial E \cap \partial E'$ be an interior face shared by E and E'. Assume that ϕ is a generic piecewise smooth function (scalar-valued or vector-valued), we define the average of ϕ on e as $\{\{\phi\}\} := \frac{1}{2}(\phi + \phi')$, where ϕ and ϕ' denote the trace of ϕ from the interior of E and E'. Let v be a piecewise smooth function and $\boldsymbol{v}$ a piecewise smooth vector-valued field. We also define the following jumps on e as

$$[\![v]\!] := v\boldsymbol{n}_E + v'\boldsymbol{n}_{E'},\ [\![\boldsymbol{v}]\!] := \boldsymbol{v}\otimes\boldsymbol{n}_E + \boldsymbol{v}'\otimes\boldsymbol{n}_{E'},$$

$$[\![\boldsymbol{v}]\!]_N := \boldsymbol{v}\cdot\boldsymbol{n}_E + \boldsymbol{v}'\cdot\boldsymbol{n}_{E'},\ [\![\boldsymbol{v}]\!]_T := \boldsymbol{v}\times\boldsymbol{n}_E + \boldsymbol{v}'\times\boldsymbol{n}_{E'}.$$

On a boundary face $e = \partial E \cap \partial\Omega$, we set accordingly $\{\{\phi\}\} := \phi$, $[\![v]\!] := v\boldsymbol{n}$, $[\![\boldsymbol{v}]\!] := \boldsymbol{v}\otimes\boldsymbol{n}$, $[\![\boldsymbol{v}]\!]_N := \boldsymbol{v}\cdot\boldsymbol{n}$ and $[\![\boldsymbol{v}]\!]_T := \boldsymbol{v}\times\boldsymbol{n}$.

For any integer $l \ge 1$, we introduce the following discrete function spaces

$$\boldsymbol{X}_h = \{\boldsymbol{v}_h \in [L^2(\Omega)]^d : \forall E \in \mathcal{E}_h,\ \boldsymbol{v}_h|_E \in [\mathbb{P}_l(E)]^d\},$$

$$\boldsymbol{Y}_h = \{\boldsymbol{w}_h \in [L^2(\Omega)]^d : \forall E \in \mathcal{E}_h,\ \boldsymbol{w}_h|_E \in [\mathbb{P}_l(E)]^d\},$$

$$\boldsymbol{V}_h = \{\boldsymbol{v}_h \in \boldsymbol{X}_h : \forall q_h \in M_h,\ \mathcal{B}(\boldsymbol{v}_h, q_h) = 0\},$$

$$M_h = \{q_h \in L^2(\Omega) : \forall E \in \mathcal{E}_h,\ q_h|_E \in \mathbb{P}_{l-1}(E)\},$$

$$\boldsymbol{W}_h = \boldsymbol{Y}_h + \boldsymbol{H}_0(curl;\Omega),$$

where $\mathbb{P}_l(E)$ is the space of polynomials of degree l on the element E, and the operator $\mathcal{B}$ will be defined as below. We make the assumption that $\boldsymbol{X}_h$ and M_h meet the requirements of the inf-sup condition (see [46]) in the sense of

$$\inf_{q\in M_h}\sup_{\boldsymbol{v}\in\boldsymbol{X}_h}\frac{\mathcal{B}(\boldsymbol{v},q)}{\|\boldsymbol{v}\|_{DG}} \ge \gamma\|q\|_{L^2(\Omega)},$$

where $\gamma > 0$ is a constant.

We also define several energy norms based on the above discontinuous Sobolev spaces as

$$\|\boldsymbol{v}\|_{DG}^2 = \sum_{E\in\mathcal{E}_h} \|\nabla \boldsymbol{v}\|_{L^2(E)}^2 + \sum_{e\in\mathcal{F}_h} \frac{\sigma_e}{h_e} \|[\![\boldsymbol{v}]\!]\|_{L^2(e)}^2, \qquad \forall \boldsymbol{v}\in \boldsymbol{X}_h,$$

$$\|\boldsymbol{w}\|_{D}^2 = \sum_{E\in\mathcal{E}_h} \|\nabla \times \boldsymbol{w}\|_{L^2(E)}^2 + \sum_{e\in\mathcal{F}_h} \frac{\sigma_e}{h_e} \|[\![\boldsymbol{w}]\!]_T\|_{L^2(e)}^2, \qquad \forall \boldsymbol{w}\in \boldsymbol{W}_h,$$

$$\|\boldsymbol{w}\|_{dG}^2 = \sum_{E\in\mathcal{E}_h} \|\boldsymbol{w}\|_{L^2(E)}^2 + \|\boldsymbol{w}\|_{D}^2, \qquad \forall \boldsymbol{w}\in \boldsymbol{W}_h,$$

$$\|\boldsymbol{w}\|_{C}^2 = \sum_{E\in\mathcal{E}_h} \|\nabla \cdot \boldsymbol{w}\|_{L^2(E)}^2 + \sum_{e\in\mathcal{F}_h} \frac{\bar{\sigma}_e}{h_e} \|[\![\boldsymbol{w}]\!]_N\|_{L^2(e)}^2, \qquad \forall \boldsymbol{w}\in \boldsymbol{W}_h,$$

$$\|q\|_{E}^2 = \sum_{E\in\mathcal{E}_h} \|\nabla q\|_{L^2(E)}^2 + \sum_{e\in\mathcal{F}_h} \frac{\tilde{\sigma}_e}{h_e} \|[\![q]\!]\|_{L^2(e)}^2, \qquad \forall q\in M_h.$$

For the approximations of the initial values, let $\boldsymbol{u}_h^0$, $\boldsymbol{m}_h^0$ be the L^2 projection of $\boldsymbol{u}^0$, $\boldsymbol{m}^0$ onto $\boldsymbol{X}_h$ and $\boldsymbol{Y}_h$, respectively, namely

$$\int_E (\boldsymbol{u}_h^0 - \boldsymbol{u}^0)\cdot \boldsymbol{v}_h = 0,\ \forall \boldsymbol{v}_h \in [\mathbb{P}_l(E)]^d,\ \int_E (\boldsymbol{m}_h^0 - \boldsymbol{m}^0)\cdot \boldsymbol{w}_h = 0,\ \forall \boldsymbol{w}_h \in [\mathbb{P}_l(E)]^d.$$

We start with setting $p_h^0 = z_h^0 = 0$ and $\tilde{\boldsymbol{u}}_h^0 = \boldsymbol{u}_h^0$, then the fully discrete DG scheme of (2.1)-(2.3) read as follows.

Step 1: Find $\boldsymbol{m}_h^{k+1} \in \boldsymbol{W}_h$ such that for all $\boldsymbol{w}_h \in \boldsymbol{W}_h$, there holds

$$\begin{aligned}&(\frac{3\boldsymbol{m}_h^{k+1} - 4\boldsymbol{m}_h^k + \boldsymbol{m}_h^{k-1}}{2\tau}, \boldsymbol{w}_h) + \nu_m \mathcal{M}(\boldsymbol{m}_h^{k+1}, \boldsymbol{w}_h) + \nu_m \mathcal{O}(\boldsymbol{m}_h^{k+1}, \boldsymbol{w}_h)\\ &\quad + C(\hat{\boldsymbol{u}}_h^*, \hat{\boldsymbol{m}}_h^*, \boldsymbol{w}_h) + \beta\tau^2 \mathcal{G}(\boldsymbol{m}_h^{k+1}, \boldsymbol{w}_h) = 0.\end{aligned} \tag{3.1}$$

Step 2: Find $\tilde{\boldsymbol{u}}_h^{k+1} \in \boldsymbol{X}_h$ such that for all $\boldsymbol{v}_h \in \boldsymbol{X}_h$, there holds

$$\begin{aligned}&(\frac{3\tilde{\boldsymbol{u}}_h^{k+1} - 4\boldsymbol{u}_h^k + \boldsymbol{u}_h^{k-1}}{2\tau}, \boldsymbol{v}_h) + \nu \mathcal{A}(\tilde{\boldsymbol{u}}_h^{k+1}, \boldsymbol{v}_h) + D(\hat{\boldsymbol{u}}_h^*, \hat{\boldsymbol{u}}_h^*, \tilde{\boldsymbol{u}}_h^{k+1}, \boldsymbol{v}_h)\\ &\quad + \mathcal{B}(\boldsymbol{v}_h, p_h^k) - \kappa C(\boldsymbol{v}_h, \hat{\boldsymbol{m}}_h^*, \boldsymbol{m}_h^{k+1}) = 0.\end{aligned} \tag{3.2}$$

Step 3: Find $z_h^{k+1} \in M_h$ such that for all $q_h \in M_h$, there holds

$$\mathcal{A}_e(z_h^{k+1}, q_h) = \frac{3}{2\tau}\mathcal{B}(\tilde{\boldsymbol{u}}_h^{k+1}, q_h). \tag{3.3}$$

Step 4: Find $(\boldsymbol{u}_h^{k+1}, p_h^{k+1}) \in (\boldsymbol{V}_h, M_h)$ such that for all $(\boldsymbol{v}_h, q_h) \in (\boldsymbol{X}_h, M_h)$, there holds

$$(\frac{3\boldsymbol{u}_h^{k+1} - 3\tilde{\boldsymbol{u}}_h^{k+1}}{2\tau}, \boldsymbol{v}_h) + \mathcal{B}(\boldsymbol{v}_h, z_h^{k+1}) = 0, \tag{3.4a}$$

$$(p_h^{k+1}, q_h) = (p_h^k, q_h) + (z_h^{k+1}, q_h) + \lambda\nu\mathcal{B}(\tilde{\boldsymbol{u}}_h^{k+1}, q_h). \tag{3.4b}$$

Similar to [2], a way to achieve second-order accuracy in the BDF2 scheme (3.1)-(3.4), we set the two initial values as $\boldsymbol{m}_h^{-1} = \boldsymbol{m}_h^0$ and $\boldsymbol{u}_h^{-1} = \boldsymbol{u}_h^0$. Note that in the DG scheme (3.1)-(3.4), we encapsulate a number of operators, such as $\mathcal{A}$, $\mathcal{A}_e$, $\mathcal{M}$, $\mathcal{O}$, C, $\mathcal{G}$, D, $\mathcal{B}$, which are described below one by one.

• **The bilinear forms $\mathcal{A}$ and $\mathcal{A}_e$**, which are for the DG discretization of the Laplace operator, and set as the standard interior penalty form defined as:

$$\begin{aligned}\mathcal{A}(\boldsymbol{u}, \boldsymbol{v}) = &\sum_{E\in\mathcal{E}_h} (\nabla \boldsymbol{u}, \nabla \boldsymbol{v})_E - \sum_{e\in\mathcal{F}_h} (\{\{\nabla \boldsymbol{u}\}\}, [\![\boldsymbol{v}]\!])_e\\ &- \sum_{e\in\mathcal{F}_h} (\{\{\nabla \boldsymbol{v}\}\}, [\![\boldsymbol{u}]\!])_e + \sum_{e\in\mathcal{F}_h} \frac{\sigma_e}{h_e} ([\![\boldsymbol{u}]\!], [\![\boldsymbol{v}]\!])_e, \forall \boldsymbol{u}, \boldsymbol{v} \in \boldsymbol{X}_h,\end{aligned}$$

and

$$\begin{aligned}\mathcal{A}_e(p, q) = &\sum_{E\in\mathcal{E}_h} (\nabla p, \nabla q)_E - \sum_{e\in\mathcal{F}_h} (\{\{\nabla p\}\}, [\![q]\!])_e\\ &- \sum_{e\in\mathcal{F}_h} (\{\{\nabla q\}\}, [\![p]\!])_e + \sum_{e\in\mathcal{F}_h} \frac{\tilde{\sigma}_e}{h_e} ([\![p]\!], [\![q]\!])_e,\ \forall p, q \in M_h,\end{aligned}$$

where $\sigma_e, \tilde{\sigma}_e > 0$ are stabilization parameters should be chosen large enough.

• **The bilinear form $\widetilde{\mathcal{M}}$ and its extension $\mathcal{M}$.** In general, for the discretization of the Maxwell operator, the form $\widetilde{\mathcal{M}}$ is used to discrete the curl-curl operator $\nabla \times (\nabla \times \boldsymbol{m})$, namely

$$\widetilde{\mathcal{M}}(\boldsymbol{m},\boldsymbol{w}) = \sum_{E\in\mathcal{E}_h}(\nabla\times\boldsymbol{m},\nabla\times\boldsymbol{w})_E - \sum_{e\in\mathcal{F}_h}(\{\{\nabla\times\boldsymbol{m}\}\},[\![\boldsymbol{w}]\!]_T)_e$$
$$- \sum_{e\in\mathcal{F}_h}(\{\{\nabla\times\boldsymbol{w}\}\},[\![\boldsymbol{m}]\!]_T)_e + \sum_{e\in\mathcal{F}_h}\frac{\sigma_e}{h_e}([\![\boldsymbol{m}]\!]_T,[\![\boldsymbol{w}]\!]_T)_e,\ \forall \boldsymbol{m},\boldsymbol{w}\in\boldsymbol{Y}_h.$$

Clearly, the form $\widetilde{\mathcal{M}}(\cdot,\cdot)$ is well-defined over $\boldsymbol{Y}_h\times\boldsymbol{Y}_h$. But, to get a better coercivity condition, we extend the form of $\widetilde{\mathcal{M}}(\cdot,\cdot)$ onto $\boldsymbol{W}_h\times\boldsymbol{W}_h$, as stated in [28,34,36], defined by

$$\mathcal{M}(\boldsymbol{m},\boldsymbol{w}) = \sum_{E\in\mathcal{E}_h}(\nabla\times\boldsymbol{m},\nabla\times\boldsymbol{w})_E - \sum_{e\in\mathcal{F}_h}(\{\{\Pi_h(\nabla\times\boldsymbol{m})\}\},[\![\boldsymbol{w}]\!]_T)_e$$
$$- \sum_{e\in\mathcal{F}_h}(\{\{\Pi_h(\nabla\times\boldsymbol{w})\}\},[\![\boldsymbol{m}]\!]_T)_e + \sum_{e\in\mathcal{F}_h}\frac{\sigma_e}{h_e}([\![\boldsymbol{m}]\!]_T,[\![\boldsymbol{w}]\!]_T)_e,\ \forall \boldsymbol{m},\boldsymbol{w}\in\boldsymbol{W}_h,$$

where Π_h denotes the standard L^2-projection onto $\boldsymbol{Y}_h$. Note that $\widetilde{\mathcal{M}}(\cdot,\cdot)$ equals $\mathcal{M}(\cdot,\cdot)$ on $\boldsymbol{Y}_h\times\boldsymbol{Y}_h$ and is well-defined on $\boldsymbol{H}_0(curl;\Omega)\times\boldsymbol{H}_0(curl;\Omega)$.

- **The trilinear form** C, which is the DG form of the coupling term, namely

$$C(\boldsymbol{u},\boldsymbol{m},\boldsymbol{w}) = -\sum_{E\in\mathcal{E}_h}(\boldsymbol{u},\boldsymbol{m}\times\nabla\times\boldsymbol{w})_E + \sum_{e\in\mathcal{F}_h}(\{\{\boldsymbol{m}\}\}\times[\![\boldsymbol{w}]\!]_T,\{\{\boldsymbol{u}\}\})_e,\ \forall \boldsymbol{u}\in\boldsymbol{X}_h,\boldsymbol{m},\boldsymbol{w}\in\boldsymbol{W}_h.$$

- **The advective term** D, which is given by the usual upwind DG formulation and reads as

$$D(\boldsymbol{z},\boldsymbol{u};\boldsymbol{v},\boldsymbol{\rho}) = \sum_{E\in\mathcal{E}_h}(\boldsymbol{u}\cdot\nabla\boldsymbol{v},\boldsymbol{\rho})_E + \frac{1}{2}\sum_{E\in\mathcal{E}_h}(\nabla\cdot\boldsymbol{u},\boldsymbol{v}\cdot\boldsymbol{\rho})_E$$
$$- \frac{1}{2}\sum_{e\in\mathcal{F}_h}([\![\boldsymbol{u}]\!],\{\{\boldsymbol{v}\cdot\boldsymbol{\rho}\}\})_e + \sum_{E\in\mathcal{E}_h}(|\{\{\boldsymbol{u}\}\}\cdot\boldsymbol{n}_E|(\boldsymbol{v}^{int}-\boldsymbol{v}^{ext}),\boldsymbol{\rho}^{int})_{\partial E^{\boldsymbol{z}}_-},$$

for $\forall \boldsymbol{z},\boldsymbol{u},\boldsymbol{v},\boldsymbol{\rho}\in\boldsymbol{X}_h$. Here, we define the inflow boundary of E as $\partial E^{\boldsymbol{z}}_- = \{\boldsymbol{x}\in\partial E : \{\{\boldsymbol{z}\}\}\cdot\boldsymbol{n}_E<0\}$, denote by $\boldsymbol{v}^{int}$ and $\boldsymbol{v}^{ext}$ the values of the trace of function $\boldsymbol{v}$ taken from the interior and exterior of E, respectively. If the edge lies on $\partial\Omega$, we have $\boldsymbol{v}^{int}=\boldsymbol{v}$ and $\boldsymbol{v}^{ext}=\boldsymbol{0}$.

- **The penalty operator** $\mathcal{O}$, which is used to approximate the divergence free condition (see Remark 3.1), and defined as

$$\mathcal{O}(\boldsymbol{m},\boldsymbol{w}) = \sum_{E\in\mathcal{E}_h}(\nabla\cdot\boldsymbol{m},\nabla\cdot\boldsymbol{w})_E + \sum_{e\in\mathcal{F}_h}\frac{\bar{\sigma}_e}{h_e}([\![\boldsymbol{m}]\!]_N,[\![\boldsymbol{w}]\!]_N)_e,$$

where the parameter $\bar{\sigma}_e>0$ must be set sufficiently high.

- **The stabilization term** $\mathcal{G}$ (see Remark 3.1), which is defined as

$$\mathcal{G}(\boldsymbol{m},\boldsymbol{w}) = \sum_{E\in\mathcal{E}_h}(\hat{\boldsymbol{m}}^*_h\times\nabla\times\boldsymbol{m},\hat{\boldsymbol{m}}^*_h\times\nabla\times\boldsymbol{w})_E + \sum_{e\in\mathcal{F}_h}\frac{\sigma_e}{h_e}(\{\{\hat{\boldsymbol{m}}^*_h\}\}\times[\![\boldsymbol{m}]\!]_T,\{\{\hat{\boldsymbol{m}}^*_h\}\}\times[\![\boldsymbol{w}]\!]_T)_e.$$

- **The lift operator** F_h**.** We further introduce the lift operator for DG method analysis in theory. By giving $e\in\mathcal{F}_h$, we construct the operator $F_h : \boldsymbol{X}_h\to M_h$ such that

$$(F_h([\![\boldsymbol{v}_h]\!]),q_h) = \sum_{e\in\mathcal{F}_h}([\![\boldsymbol{v}_h]\!]_N,\{\{q_h\}\})_e,\ \forall \boldsymbol{v}_h\in\boldsymbol{X}_h,q_h\in M_h. \tag{3.5}$$

It is easy to check that F_h is a linear operator (see [17,42]). One can also obtain the bound for the lift operator F_h in (3.5) (cf. [35,42]), namely,

$$\|F_h([\![\boldsymbol{v}_h]\!])\| \le \tilde{C}_k\Big(\sum_{e\in\mathcal{F}_h}h_e^{-1}\|[\![\boldsymbol{v}_h]\!]\|^2_{L^2(e)}\Big)^{1/2},\ \forall \boldsymbol{v}_h\in\boldsymbol{X}_h, \tag{3.6}$$

where $\tilde{C}_k>0$ is a constant independent of h and τ.

- **The bilinear term** $\mathcal{B}$, which is related to the discretization of the gradient and divergence operator (e.g. ∇p and $-\nabla\cdot\boldsymbol{v}$), and is defined as

$$\mathcal{B}(\boldsymbol{v},q) = -\sum_{E\in\mathcal{E}_h}(\nabla\cdot\boldsymbol{v},q)_E + \sum_{e\in\mathcal{F}_h}([\![\boldsymbol{v}]\!]_N,\{\{q\}\})_e,\ \forall \boldsymbol{v}\in\boldsymbol{X}_h,q\in M_h.$$

Using the lift operator, we have the following equivalent form to $\mathcal{B}(\boldsymbol{v}_h,q_h)$:

$$\mathcal{B}(\boldsymbol{v}_h,q_h) = -(\nabla_h\cdot\boldsymbol{v}_h,q_h) + (F_h([\![\boldsymbol{v}_h]\!]),q_h), \tag{3.7}$$

for all $\boldsymbol{v}_h\in\boldsymbol{X}_h,q_h\in M_h$, where $\nabla_h\cdot$ denotes the broken divergence operator.

The following remark provides a detailed explanation of the construction strategy employed in developing the scheme (3.1)-(3.4).

Remark 3.1.

- In (3.1), we handle the coupled nonlinear term (in the trilinear form C) by extrapolating the variables $\boldsymbol{m}$ and $\boldsymbol{u}$. This explicit treatment helps us to obtain linear and decoupled computations. In (3.2)-(3.4), we make use of the pressure-correction method with second-order time accuracy for solving the Navier-Stokes system. This method enables the computation of the velocity field and the pressure to be decoupled. In (3.4b), $\lambda = 0$ yields the standard forms of pressure-correction projection method (cf. [22]), whereas $\lambda = 1$ yields the rotational pressure-correction form (cf. [29,30]).
- In (3.1), we incorporate a penalty term $\nu_m \mathcal{O}(\boldsymbol{m}_h^{k+1}, \boldsymbol{w}_h)$ to approximate the exact penalty formulation for the magnetic field in the spatial discrete case (see also in [5,56]). We also add an additional stabilization term $\beta\tau^2\mathcal{G}$ artificially, which plays a crucial role in balancing the explicit treatment for the nonlinear coupling term $\nabla\times(\boldsymbol{u}\times\boldsymbol{m})$ (see term C) in (3.1), and $\beta > 0$ is an artificial parameter. The stabilization term $\beta\tau^2\mathcal{G}$ can be treated as a second-order perturbation to the equation (2.4a) at the discrete level, then it leads to an additional consistency error of second-order $\mathcal{O}(\tau^2)$ which has the same order as the error introduced by the explicit treatment of coupling term. Similar stabilization techniques can be found in [48,49] for the phase-field type equations.

Remark 3.2.

- If we adopt the stabilized Gauge-Uzawa method [44] for solving the MHD system, the Step 3 and Step 4 will become the following steps:
  Step 3: Find $\psi_h^{k+1} \in M_h$ such that for all $q_h \in M_h$, there holds

$$\mathcal{A}_e(\psi_h^{k+1}, q_h) = \mathcal{A}_e(\psi_h^k, q_h) - \mathcal{B}(\tilde{\boldsymbol{u}}_h^{k+1}, q_h).$$

  Step 4: Find $(\boldsymbol{u}_h^{k+1}, z_h^{k+1}) \in (\boldsymbol{V}_h, M_h)$ such that for all $(\boldsymbol{v}_h, q_h) \in (\boldsymbol{X}_h, M_h)$, there holds

$$(\boldsymbol{u}_h^{k+1} - \tilde{\boldsymbol{u}}_h^{k+1}, \boldsymbol{v}_h) - \mathcal{B}(\boldsymbol{v}_h, \psi_h^{k+1} - \psi_h^k) = 0,$$
$$(z_h^{k+1}, q_h) = (z_h^k, q_h) + \lambda\nu\mathcal{B}(\tilde{\boldsymbol{u}}_h^{k+1}, q_h).$$

  Step 5: Update p_h^{k+1} by

$$p_h^{k+1} = -\frac{3\psi_h^{k+1}}{2\tau} + \nu z_h^{k+1}.$$

  Note that, the similar stability results can be proved by using the same argument as the proof of rotational pressure-correction scheme at a later.
- Compared with the decoupled schemes developed in [40,57], we don't need to reformulate the MHD system, each equation in the original system can be solved independently. More precisely, in [40], the implicit-explicit schemes are constructed based on the scalar auxiliary variable approach for the MHD system, its require solving a sequence of linear differential equations with constant coefficients at each time step. In [57], the MHD system is reformulated by the "zero-energy-contribution" characteristics, a nonlocal scalar variable and its corresponding ordinary differential equation should be solved at each time step.
- We also remark that, the optimal rate convergence analysis and error estimate of the proposed numerical scheme is not derived theoretically here, but it will be considered in our ongoing work. The interested readers can refer to the related works in [44,61,62], or the numerical analysis for certain coupled physical system, such as a phase-field models for two-phase incompressible flows, see the existing works in [9,10,18,20,21,41,52].

3.2. Well-posedness

In the subsequent, we will first review and prove a number of conclusions that are already common knowledge about the DG formulations, and demonstrate the well-posedness of our developed scheme.

Lemma 3.3. *The bilinear forms $\mathcal{A}$, $\mathcal{M}$, and $\mathcal{A}_e$ satisfy the conditions as follows,*

$$\mathcal{A}(\boldsymbol{u}, \boldsymbol{v}) \le C_1\|\boldsymbol{u}\|_{DG}\|\boldsymbol{v}\|_{DG},\ \mathcal{A}(\boldsymbol{v}, \boldsymbol{v}) \ge K_1\|\boldsymbol{v}\|_{DG}^2,\ \forall \boldsymbol{u}, \boldsymbol{v} \in \boldsymbol{X}_h, \tag{3.8}$$

$$\mathcal{M}(\boldsymbol{m}, \boldsymbol{w}) \le C_2\|\boldsymbol{m}\|_D\|\boldsymbol{w}\|_D,\ \mathcal{M}(\boldsymbol{w}, \boldsymbol{w}) \ge K_2\|\boldsymbol{w}\|_D^2,\ \forall \boldsymbol{m}, \boldsymbol{w} \in \boldsymbol{W}_h, \tag{3.9}$$

$$\mathcal{A}_e(p, q) \le C_3\|p\|_E\|q\|_E,\ \mathcal{A}_e(q, q) \ge K_3\|q\|_E^2,\ \forall p, q \in M_h, \tag{3.10}$$

where $C_i, K_i, i = 1, 2, 3$ are positive constants.

Proof. For a detailed proof, please refer to [26,28,46]. □

Based on the coercivity of $\mathcal{A}$, $\mathcal{M}$, and $\mathcal{A}_e$, it can be inferred that these operators are non-negative. For the sake of convenience, the following broken energy norms are also defined:

$$
\begin{aligned}
&|||\boldsymbol{v}|||_{DG}^2 = \mathcal{A}(\boldsymbol{v},\boldsymbol{v}) \geq 0,\\
&|||\boldsymbol{w}|||_{D}^2 = \mathcal{M}(\boldsymbol{w},\boldsymbol{w}) \geq 0,\\
&|||q|||_{E}^2 = \mathcal{A}_e(q,q) \geq 0,
\end{aligned}
\tag{3.11}
$$

which will be used repeatedly in the subsequent analysis.

Lemma 3.4. *There exists a positive constant C_e such that the form C satisfies*

$$
C(\boldsymbol{u},\boldsymbol{m},\boldsymbol{w}) \leq C_e \|\boldsymbol{u}\|_{L^2(\Omega)} \|\boldsymbol{m}\times\nabla\times\boldsymbol{w}\|_{\mathcal{G}},\ \forall \boldsymbol{u}\in\boldsymbol{X}_h, \boldsymbol{m},\boldsymbol{w}\in\boldsymbol{W}_h,
\tag{3.12}
$$

where the norm $\|\cdot\|_{\mathcal{G}}$ is defined by

$$
\|\boldsymbol{m}\times\nabla\times\boldsymbol{w}\|_{\mathcal{G}} = \Big(\sum_{E\in\mathcal{E}_h} \|\boldsymbol{m}\times\nabla\times\boldsymbol{w}\|_{L^2(E)}^2 + \sum_{e\in\mathcal{F}_h} \frac{\sigma_e}{h_e} \|\{\{\boldsymbol{m}\}\}\times[\![\boldsymbol{w}]\!]_T\|_{L^2(e)}^2\Big)^{\frac{1}{2}}.
$$

.

Proof. From the Cauchy-Schwarz inequality, Hölder inequality and trace inequality (see [46]), we derive

$$
\begin{aligned}
C(\boldsymbol{u},\boldsymbol{m},\boldsymbol{w}) &\leq \Big(\sum_{E\in\mathcal{E}_h} \|\boldsymbol{u}\|_{L^2(E)}^2\Big)^{\frac{1}{2}} \Big(\sum_{E\in\mathcal{E}_h} \|\boldsymbol{m}\times\nabla\times\boldsymbol{w}\|_{L^2(E)}^2\Big)^{\frac{1}{2}}\\
&\quad + \Big(\sum_{e\in\mathcal{F}_h} \|\{\{\boldsymbol{m}\}\}\times[\![\boldsymbol{w}]\!]_T\|_{L^2(e)}^2\Big)^{\frac{1}{2}} \Big(\sum_{e\in\mathcal{F}_h} \|\{\{\boldsymbol{u}\}\}\|_{L^2(e)}^2\Big)^{\frac{1}{2}}\\
&\leq \Big(\sum_{E\in\mathcal{E}_h} \|\boldsymbol{u}\|_{L^2(E)}^2\Big)^{\frac{1}{2}} \Big(\sum_{E\in\mathcal{E}_h} \|\boldsymbol{m}\times\nabla\times\boldsymbol{w}\|_{L^2(E)}^2\Big)^{\frac{1}{2}}\\
&\quad + \frac{C}{\sigma_e^{1/2}} \Big(\sum_{E\in\mathcal{E}_h} \|\boldsymbol{u}\|_{L^2(E)}^2\Big)^{\frac{1}{2}} \Big(\sum_{e\in\mathcal{F}_h} \frac{\sigma_e}{h_e} \|\{\{\boldsymbol{m}\}\}\times[\![\boldsymbol{w}]\!]_T\|_{L^2(e)}^2\Big)^{\frac{1}{2}},
\end{aligned}
$$

which implies the conclusion. □

Lemma 3.5. *The form $\mathcal{D}$ satisfies the following continuity result*

$$
\mathcal{D}(\boldsymbol{z},\boldsymbol{u};\boldsymbol{v},\boldsymbol{\rho}) \leq C_4 \|\boldsymbol{u}\|_{DG} \|\boldsymbol{v}\|_{DG} \|\boldsymbol{\rho}\|_{DG},
$$

for all $\boldsymbol{z},\boldsymbol{u},\boldsymbol{v},\boldsymbol{\rho}\in\boldsymbol{X}_h$, where $C_4>0$ is a constant.

Proof. For a detailed proof, please refer to [27,46,61]. □

Lemma 3.6. *The form $\mathcal{D}$ satisfies the following positivity property*

$$
\mathcal{D}(\boldsymbol{u},\boldsymbol{u};\boldsymbol{v},\boldsymbol{v}) = \frac{1}{2} \sum_{E\in\mathcal{E}_h} \||\{\{\boldsymbol{u}\}\}\cdot\boldsymbol{n}_E|^{1/2} (\boldsymbol{v}^{int}-\boldsymbol{v}^{ext})\|_{L^2(\partial E^{\boldsymbol{u}}_{-}\setminus\partial\Omega)}^2 + \||\boldsymbol{u}\cdot\boldsymbol{n}|^{1/2}\boldsymbol{v}\|_{L^2(\partial\Omega^{\boldsymbol{v}}_{+})}^2 \geq 0,
$$

for all $\boldsymbol{u},\boldsymbol{v}\in\boldsymbol{X}_h$.

Proof. For a detailed proof, please refer to [27,46]. □

Now, the well-posedness of the proposed scheme (3.1)-(3.4) is stated as the following theorem.

Theorem 3.7. *The decoupled scheme (3.1)-(3.4) admits a unique solution $(\boldsymbol{m}_h^{k+1},\boldsymbol{u}_h^{k+1},p_h^{k+1})\in\boldsymbol{W}_h\times\boldsymbol{X}_h\times M_h$.*

Proof. (i) First, we show the well-posedness of (3.1) in step 1. We define a bilinear form $\mathcal{F}_1(\cdot,\cdot):\boldsymbol{W}_h\times\boldsymbol{W}_h\to\mathbb{R}$ by

$$
\mathcal{F}_1(\boldsymbol{m},\boldsymbol{w}) = \frac{3}{2\tau}(\boldsymbol{m},\boldsymbol{w}) + \nu_m\mathcal{M}(\boldsymbol{m},\boldsymbol{w}) + \nu_m\mathcal{O}(\boldsymbol{m},\boldsymbol{w}) + \beta\tau^2\mathcal{G}(\boldsymbol{m},\boldsymbol{w}),
$$

and a linear form $L_1(\cdot):\boldsymbol{W}_h\to\mathbb{R}$ is given by

$$
L_1(\boldsymbol{w}) = \frac{1}{2\tau}(4\boldsymbol{m}_h^k - \boldsymbol{m}_h^{k-1},\boldsymbol{w}) - C(\hat{\boldsymbol{u}}_h^*,\hat{\boldsymbol{m}}_h^*,\boldsymbol{w}).
$$

Therefore, the first step (3.1) can be expressed as: find $\boldsymbol{m}_h^{k+1}\in\boldsymbol{W}_h$ such that for all $\boldsymbol{w}_h\in\boldsymbol{W}_h$, there holds

$$
\mathcal{F}_1(\boldsymbol{m}_h^{k+1},\boldsymbol{w}_h) = L_1(\boldsymbol{w}_h).
$$

By using Lemma 3.3, we can easily check that the form $\mathcal{F}_1(\cdot,\cdot)$ is continues and coercive, namely

$$\begin{aligned}\mathcal{F}_1(\boldsymbol{m},\boldsymbol{w}) &\le \frac{3}{2\tau}\|\boldsymbol{m}\|\|\boldsymbol{w}\| + C_2\nu_m\|\boldsymbol{m}\|_D\|\boldsymbol{w}\|_D + \nu_m\|\boldsymbol{m}\|_C\|\boldsymbol{w}\|_C + \beta\tau^2\|\hat{\boldsymbol{m}}_h^*\|^2_{L^\infty(\Omega)}\|\boldsymbol{m}\|_D\|\boldsymbol{w}\|_D \\ &\le C_5\|\boldsymbol{m}\|_{dG}\|\boldsymbol{w}\|_{dG},\end{aligned}$$

and

$$\mathcal{F}_1(\boldsymbol{m},\boldsymbol{m}) \ge \frac{3}{2\tau}\|\boldsymbol{m}\|^2 + K_2\nu_m\|\boldsymbol{m}\|_D^2 + \nu_m\|\boldsymbol{m}\|_C^2 + \beta\tau^2\|\hat{\boldsymbol{m}}_h^*\times\nabla\times\boldsymbol{m}\|_{\mathcal{G}}^2 \ge C_6\|\boldsymbol{m}\|_{dG}^2,$$

where $C_5>0$ and $C_6>0$ are two constants. Thus, by using the Lax-Milgram theorem, we can derive that the equation (3.1) has a unique solution $\boldsymbol{m}_h^{k+1}\in\boldsymbol{W}_h$.

(ii) We show the well-posedness of (3.2) in step 2. We define a bilinear form $\mathcal{F}_2(\cdot,\cdot):\boldsymbol{X}_h\times\boldsymbol{X}_h\to\mathbb{R}$ by

$$\mathcal{F}_2(\boldsymbol{u},\boldsymbol{v}) = \frac{3}{2\tau}(\boldsymbol{u},\boldsymbol{v}) + \nu\mathcal{A}(\boldsymbol{u},\boldsymbol{v}) + \mathcal{D}(\hat{\boldsymbol{u}}_h^*,\hat{\boldsymbol{u}}_h^*,\boldsymbol{u},\boldsymbol{v}),$$

and a linear form $L_2(\cdot):\boldsymbol{X}_h\to\mathbb{R}$ by

$$L_2(\boldsymbol{v}) = \frac{1}{2\tau}(4\boldsymbol{u}_h^k - \boldsymbol{u}_h^{k-1},\boldsymbol{v}) - \mathcal{B}(\boldsymbol{v},p_h^k) + \kappa\mathcal{C}(\boldsymbol{v},\hat{\boldsymbol{m}}_h^*,\boldsymbol{m}_h^{k+1}).$$

Then, the second step (3.2) can be rewritten as: Find $\tilde{\boldsymbol{u}}_h^{k+1}\in\boldsymbol{X}_h$ such that for all $\boldsymbol{v}_h\in\boldsymbol{X}_h$, there holds

$$\mathcal{F}_2(\tilde{\boldsymbol{u}}_h^{k+1},\boldsymbol{v}_h) = L_2(\boldsymbol{v}_h).$$

Making use of Lemma 3.5, Lemma 3.6 and Lemma 3.3, we can prove that $\mathcal{F}_2(\cdot,\cdot)$ is bounded and coercive, namely

$$\mathcal{F}_2(\boldsymbol{u},\boldsymbol{v}) \le \frac{3}{2\tau}\|\boldsymbol{u}\|\|\boldsymbol{v}\| + C_1\nu\|\boldsymbol{u}\|_{DG}\|\boldsymbol{v}\|_{DG} + C_4\|\hat{\boldsymbol{u}}_h^*\|_{DG}\|\boldsymbol{u}\|_{DG}\|\boldsymbol{v}\|_{DG} \le C_7\|\boldsymbol{u}\|_{DG}\|\boldsymbol{v}\|_{DG},$$

and

$$\mathcal{F}_2(\boldsymbol{u},\boldsymbol{u}) \ge \frac{3}{2\tau}\|\boldsymbol{u}\|^2 + K_1\nu\|\boldsymbol{u}\|_{DG}^2 \ge K_1\nu\|\boldsymbol{u}\|_{DG}^2,$$

where $C_7>0$ is a constant depends on τ, ν and $\|\hat{\boldsymbol{u}}_h^*\|_{DG}$. Therefore, we conclude that (3.2) admits a unique solution $\tilde{\boldsymbol{u}}_h^{k+1}\in\boldsymbol{X}_h$ from the Lax-Milgram theorem.

(iii) The existence and uniqueness of $\boldsymbol{u}_h^{k+1}\in\boldsymbol{X}_h$ and $p_h^{k+1}\in M_h$ can also be demonstrated by following a similar approach to (3.3) in step 3 and (3.4) in step 4, and as the proof procedure is very similar, we omit it for brevity. □

3.3. Energy stability

Some auxiliary variables are introduced here for the purpose of demonstrating energy stability. Define $S_h^0=0$ and $\psi_h^0=0$, for any $1\le k\le N$, the auxiliary functions $S_h^k\in M_h$ and $\psi_h^k\in M_h$ are given by

$$\begin{cases} S_h^k = \lambda\nu\sum_{j=1}^{k}(\nabla_h\cdot\tilde{\boldsymbol{u}}_h^j - F_h([\![\tilde{\boldsymbol{u}}_h^j]\!])), \\ \psi_h^k = p_h^k + S_h^k. \end{cases} \tag{3.13}$$

Furthermore, thanks to (3.7), the equation (3.4b) can be rewritten as

$$p_h^{k+1} = p_h^k + z_h^{k+1} - \lambda\nu(\nabla_h\cdot\tilde{\boldsymbol{u}}_h^{k+1} - F_h([\![\tilde{\boldsymbol{u}}_h^{k+1}]\!])). \tag{3.14}$$

The following two identities will be used repeatedly

$$2(a-b)a = |a|^2 - |b|^2 + |a-b|^2,\ 2(a-b)b = |a|^2 - |b|^2 - |a-b|^2, \tag{3.15}$$

$$2(3a-4b+c)a = |a|^2 - |b|^2 + |2a-b|^2 - |2b-c|^2 + |a-2b+c|^2. \tag{3.16}$$

Now, we will prove that the decoupled scheme defined in (3.1)-(3.4) possesses the energy stability, which can be demonstrated in the following way.

Theorem 3.8. *It can be shown that the scheme defined by (3.1)-(3.4) is unconditionally energy stable, in sense that*

$$\mathbb{E}_{tot}^h(\boldsymbol{m}_h^{k+1},\boldsymbol{u}_h^{k+1},\psi_h^{k+1},S_h^{k+1}) \le \mathbb{E}_{tot}^h(\boldsymbol{m}_h^k,\boldsymbol{u}_h^k,\psi_h^k,S_h^k), \tag{3.17}$$

where the discrete energy $\mathbb{E}_{tot}^h$ is defined as

$$\mathbb{E}^h_{tot}(\boldsymbol{m}_h^k,\boldsymbol{u}_h^k,\psi_h^k,S_h^k)=\frac{\kappa}{2}\|\boldsymbol{m}_h^k\|^2+\frac{\kappa}{2}\|2\boldsymbol{m}_h^k-\boldsymbol{m}_h^{k-1}\|^2+\frac{1}{2}\|\boldsymbol{u}_h^k\|^2+\frac{1}{2}\|2\boldsymbol{u}_h^k-\boldsymbol{u}_h^{k-1}\|^2 + \frac{2\tau^2}{3}|||\psi_h^k|||_E^2+\frac{\tau}{\lambda\nu}\|S_h^k\|^2.$$

Proof. By setting $\boldsymbol{w}_h=2\kappa\tau\boldsymbol{m}_h^{k+1}$ in (3.1), using (3.11) and (3.16), we obtain

$$\begin{aligned}&\frac{\kappa}{2}(\|\boldsymbol{m}_h^{k+1}\|^2-\|\boldsymbol{m}_h^k\|^2)+\frac{\kappa}{2}(\|2\boldsymbol{m}_h^{k+1}-\boldsymbol{m}_h^k\|^2-\|2\boldsymbol{m}_h^k-\boldsymbol{m}_h^{k-1}\|^2)\\&\quad+\frac{\kappa}{2}\|\boldsymbol{m}_h^{k+1}-2\boldsymbol{m}_h^k+\boldsymbol{m}_h^{k+1}\|^2+2\kappa\nu_m\tau|||\boldsymbol{m}_h^{k+1}|||_D^2+2\kappa\nu_m\tau\|\boldsymbol{m}_h^{k+1}\|_C^2\\&\quad+2\beta\kappa\tau^3\|\hat{\boldsymbol{m}}_h^*\times\nabla\times\boldsymbol{m}_h^{k+1}\|_G^2+2\kappa\tau\mathcal{C}(\hat{\boldsymbol{u}}_h^*,\hat{\boldsymbol{m}}_h^*,\boldsymbol{m}_h^{k+1})=0.\end{aligned}\tag{3.18}$$

By setting $\boldsymbol{v}_h=2\tau\tilde{\boldsymbol{u}}_h^{k+1}$ in (3.2), we can obtain

$$\begin{aligned}&(3\tilde{\boldsymbol{u}}_h^{k+1}-4\boldsymbol{u}_h^k+\boldsymbol{u}_h^{k-1},\tilde{\boldsymbol{u}}_h^{k+1})+2\nu\tau|||\tilde{\boldsymbol{u}}_h^{k+1}|||_{DG}^2+2\tau\mathcal{D}(\hat{\boldsymbol{u}}_h^*,\hat{\boldsymbol{u}}_h^*,\tilde{\boldsymbol{u}}_h^{k+1},\tilde{\boldsymbol{u}}_h^{k+1})\\&\quad+2\tau\mathcal{B}(\tilde{\boldsymbol{u}}_h^{k+1},p_h^k)-2\kappa\tau\mathcal{C}(\tilde{\boldsymbol{u}}_h^{k+1},\hat{\boldsymbol{m}}_h^*,\boldsymbol{m}_h^{k+1})=0.\end{aligned}\tag{3.19}$$

By setting $\boldsymbol{v}_h=3\boldsymbol{u}_h^{k+1}-4\boldsymbol{u}_h^k+\boldsymbol{u}_h^{k-1}$ in (3.4a), and using the fact that $\mathcal{B}(\boldsymbol{u}_h^{k+1},q_h)=0$ due to $\boldsymbol{u}_h^{k+1}\in\boldsymbol{V}_h$, we have

$$\frac{3}{2\tau}(\boldsymbol{u}_h^{k+1}-\tilde{\boldsymbol{u}}_h^{k+1},3\boldsymbol{u}_h^{k+1}-4\boldsymbol{u}_h^k+\boldsymbol{u}_h^{k-1})=-\mathcal{B}(3\boldsymbol{u}_h^{k+1}-4\boldsymbol{u}_h^k+\boldsymbol{u}_h^{k-1},z_h^{k+1})=0.\tag{3.20}$$

Thus, by using (3.15)-(3.16) and (3.20), we obtain

$$\begin{aligned}&(3\tilde{\boldsymbol{u}}_h^{k+1}-4\boldsymbol{u}_h^k+\boldsymbol{u}_h^{k-1},\tilde{\boldsymbol{u}}_h^{k+1})=(3\boldsymbol{u}_h^{k+1}-4\boldsymbol{u}_h^k+\boldsymbol{u}_h^{k-1},\boldsymbol{u}_h^{k+1})\\&\quad+(3\boldsymbol{u}_h^{k+1}-4\boldsymbol{u}_h^k+\boldsymbol{u}_h^{k-1},\tilde{\boldsymbol{u}}_h^{k+1}-\boldsymbol{u}_h^{k+1})+(3\tilde{\boldsymbol{u}}_h^{k+1}-3\boldsymbol{u}_h^{k+1},\tilde{\boldsymbol{u}}_h^{k+1})\\&=\frac{1}{2}(\|\boldsymbol{u}_h^{k+1}\|^2-\|\boldsymbol{u}_h^k\|^2+\|2\boldsymbol{u}_h^{k+1}-\boldsymbol{u}_h^k\|^2-\|2\boldsymbol{u}_h^k-\boldsymbol{u}_h^{k-1}\|^2+\|\boldsymbol{u}_h^{k+1}-2\boldsymbol{u}_h^k+\boldsymbol{u}_h^{k-1}\|^2)\\&\quad+\frac{3}{2}(\|\tilde{\boldsymbol{u}}_h^{k+1}\|^2-\|\boldsymbol{u}_h^{k+1}\|^2+\|\tilde{\boldsymbol{u}}_h^{k+1}-\boldsymbol{u}_h^{k+1}\|^2).\end{aligned}\tag{3.21}$$

From (3.19) and (3.21), we derive

$$\begin{aligned}&\frac{1}{2}(\|\boldsymbol{u}_h^{k+1}\|^2-\|\boldsymbol{u}_h^k\|^2+\|2\boldsymbol{u}_h^{k+1}-\boldsymbol{u}_h^k\|^2-\|2\boldsymbol{u}_h^k-\boldsymbol{u}_h^{k-1}\|^2+\|\boldsymbol{u}_h^{k+1}-2\boldsymbol{u}_h^k+\boldsymbol{u}_h^{k-1}\|^2)\\&\quad+\frac{3}{2}(\|\tilde{\boldsymbol{u}}_h^{k+1}\|^2-\|\boldsymbol{u}_h^{k+1}\|^2+\|\tilde{\boldsymbol{u}}_h^{k+1}-\boldsymbol{u}_h^{k+1}\|^2)+2\nu\tau|||\tilde{\boldsymbol{u}}_h^{k+1}|||_{DG}^2\\&\quad+2\tau\mathcal{D}(\hat{\boldsymbol{u}}_h^*,\hat{\boldsymbol{u}}_h^*,\tilde{\boldsymbol{u}}_h^{k+1},\tilde{\boldsymbol{u}}_h^{k+1})+2\tau\mathcal{B}(\tilde{\boldsymbol{u}}_h^{k+1},p_h^k)-2\kappa\tau\mathcal{C}(\tilde{\boldsymbol{u}}_h^{k+1},\hat{\boldsymbol{m}}_h^*,\boldsymbol{m}_h^{k+1})=0.\end{aligned}\tag{3.22}$$

By setting $\boldsymbol{v}_h=2\tau\tilde{\boldsymbol{u}}_h^{k+1}$ in (3.4a) and from (3.15), we get

$$\frac{3}{2}(\|\boldsymbol{u}_h^{k+1}\|^2-\|\tilde{\boldsymbol{u}}_h^{k+1}\|^2-\|\boldsymbol{u}_h^{k+1}-\tilde{\boldsymbol{u}}_h^{k+1}\|^2)+2\tau\mathcal{B}(\tilde{\boldsymbol{u}}_h^{k+1},z_h^{k+1})=0.\tag{3.23}$$

We rewrite (3.4a) as

$$(\tilde{\boldsymbol{u}}_h^{k+1}-\hat{\boldsymbol{u}}_h^*,\boldsymbol{v}_h)-(\boldsymbol{u}_h^{k+1}-\hat{\boldsymbol{u}}_h^*,\boldsymbol{v}_h)=\frac{2\tau}{3}\mathcal{B}(\boldsymbol{v}_h,z_h^{k+1}).\tag{3.24}$$

By setting $\boldsymbol{v}_h=\tilde{\boldsymbol{u}}_h^{k+1}-\hat{\boldsymbol{u}}_h^*$ in (3.24), using the fact that $\mathcal{B}(\hat{\boldsymbol{u}}_h^*,z_h^{k+1})=0$, we deduce

$$\|\tilde{\boldsymbol{u}}_h^{k+1}-\hat{\boldsymbol{u}}_h^*\|^2-(\boldsymbol{u}_h^{k+1}-\hat{\boldsymbol{u}}_h^*,\tilde{\boldsymbol{u}}_h^{k+1}-\hat{\boldsymbol{u}}_h^*)=\frac{2\tau}{3}\mathcal{B}(\tilde{\boldsymbol{u}}_h^{k+1},z_h^{k+1}).\tag{3.25}$$

By setting $q_h=\frac{8\tau^2}{9}z_h^{k+1}$ in (3.3) and using (3.11), we obtain

$$\frac{8\tau^2}{9}|||z_h^{k+1}|||_E^2=\frac{4\tau}{3}\mathcal{B}(\tilde{\boldsymbol{u}}_h^{k+1},z_h^{k+1}).\tag{3.26}$$

To deal with the term $\mathcal{B}(\tilde{\boldsymbol{u}}_h^{k+1},p_h^k)$ in (3.22), using the definition of ψ_h^k in (3.13), we have

$$2\tau\mathcal{B}(\tilde{\boldsymbol{u}}_h^{k+1},p_h^k)=2\tau\mathcal{B}(\tilde{\boldsymbol{u}}_h^{k+1},\psi_h^k)-2\tau\mathcal{B}(\tilde{\boldsymbol{u}}_h^{k+1},S_h^k).\tag{3.27}$$

Using the definition of S_h^k in (3.13), we obtain

$$S_h^{k+1}-S_h^k=\lambda\nu(\nabla_h\cdot\tilde{\boldsymbol{u}}_h^{k+1}-F_h([\![\tilde{\boldsymbol{u}}_h^{k+1}]\!])).\tag{3.28}$$

Using (3.14) and (3.28), it is easy to check that

$$\psi_h^{k+1}-\psi_h^k=(p_h^{k+1}-p_h^k)+(S_h^{k+1}-S_h^k)=z_h^{k+1}.\tag{3.29}$$

By setting $q_h=\psi_h^k$ in (3.3), since $\mathcal{A}_e(\cdot,\cdot)$ is symmetric, and using (3.15) and (3.29), we have

$$
\begin{aligned}
2\tau\mathcal{B}(\tilde{\boldsymbol{u}}_h^{k+1},\psi_h^k) &= \frac{4\tau^2}{3}\mathcal{A}_e(\psi_h^{k+1}-\psi_h^k,\psi_h^k)\\
&= \frac{2\tau^2}{3}(|||\psi_h^{k+1}|||_E^2-|||\psi_h^k|||_E^2-|||\psi_h^{k+1}-\psi_h^k|||_E^2)\\
&= \frac{2\tau^2}{3}(|||\psi_h^{k+1}|||_E^2-|||\psi_h^k|||_E^2)-\frac{2\tau^2}{3}|||z_h^{k+1}|||_E^2.
\end{aligned}
\tag{3.30}
$$

For the second term on the right-hand side of (3.27), by using (3.7), (3.15) and (3.28), we deduce

$$
\begin{aligned}
-2\tau\mathcal{B}(\tilde{\boldsymbol{u}}_h^{k+1},S_h^k) &= 2\tau(\nabla_h\cdot\tilde{\boldsymbol{u}}_h^{k+1}-F_h([\![\tilde{\boldsymbol{u}}_h^{k+1}]\!]),S_h^k)\\
&= \frac{2\tau}{\lambda\nu}(S_h^{k+1}-S_h^k,S_h^k)\\
&= \frac{\tau}{\lambda\nu}(\|S_h^{k+1}\|^2-\|S_h^k\|^2-\|S_h^{k+1}-S_h^k\|^2).
\end{aligned}
\tag{3.31}
$$

By substituting (3.30) and (3.31) into (3.27), we obtain

$$
\begin{aligned}
2\tau\mathcal{B}(\tilde{\boldsymbol{u}}_h^{k+1},p_h^k) &= \frac{2\tau^2}{3}(|||\psi_h^{k+1}|||_E^2-|||\psi_h^k|||_E^2)-\frac{2\tau^2}{3}|||z_h^{k+1}|||_E^2\\
&\quad+\frac{\tau}{\lambda\nu}(\|S_h^{k+1}\|^2-\|S_h^k\|^2-\|S_h^{k+1}-S_h^k\|^2).
\end{aligned}
\tag{3.32}
$$

By combining (3.18), (3.22)-(3.23), (3.25)-(3.26) with (3.32), and using Lemma 3.3 and Lemma 3.6, we arrive at

$$
\begin{aligned}
&\frac{\kappa}{2}(\|\boldsymbol{m}_h^{k+1}\|^2-\|\boldsymbol{m}_h^k\|^2)+\frac{\kappa}{2}(\|2\boldsymbol{m}_h^{k+1}-\boldsymbol{m}_h^k\|^2-\|2\boldsymbol{m}_h^k-\boldsymbol{m}_h^{k-1}\|^2)\\
&+\frac{1}{2}(\|\boldsymbol{u}_h^{k+1}\|^2-\|\boldsymbol{u}_h^k\|^2)+\frac{1}{2}(\|2\boldsymbol{u}_h^{k+1}-\boldsymbol{u}_h^k\|^2-\|2\boldsymbol{u}_h^k-\boldsymbol{u}_h^{k-1}\|^2)\\
&+\frac{2\tau^2}{3}(|||\psi_h^{k+1}|||_E^2-|||\psi_h^k|||_E^2)+\frac{\tau}{\lambda\nu}(\|S_h^{k+1}\|^2-\|S_h^k\|^2)\\
&+\frac{\kappa}{2}\|\boldsymbol{m}_h^{k+1}-2\boldsymbol{m}_h^k+\boldsymbol{m}_h^{k+1}\|^2+\frac{1}{2}\|\boldsymbol{u}_h^{k+1}-2\boldsymbol{u}_h^k+\boldsymbol{u}_h^{k-1}\|^2\\
&+\|\tilde{\boldsymbol{u}}_h^{k+1}-2\boldsymbol{u}_h^k+\boldsymbol{u}_h^{k-1}\|^2+2K_1\nu\tau\|\tilde{\boldsymbol{u}}_h^{k+1}\|_{DG}^2+2\kappa\nu_m\tau|||\boldsymbol{m}_h^{k+1}|||_D^2\\
&+2\kappa\nu_m\tau\|\boldsymbol{m}_h^{k+1}\|_C^2+\frac{2\tau^2}{9}|||z_h^{k+1}|||_E^2+2\beta\kappa\tau^3\|\hat{\boldsymbol{m}}_h^*\times\nabla\times\boldsymbol{m}_h^{k+1}\|_{\mathcal{G}}^2\\
&\le(\boldsymbol{u}_h^{k+1}-\hat{\boldsymbol{u}}_h^*,\tilde{\boldsymbol{u}}_h^{k+1}-\hat{\boldsymbol{u}}_h^*)+2\kappa\tau C(\tilde{\boldsymbol{u}}_h^{k+1}-\hat{\boldsymbol{u}}_h^*,\hat{\boldsymbol{m}}_h^k,\boldsymbol{m}_h^{k+1})+\frac{\tau}{\lambda\nu}\|S_h^{k+1}-S_h^k\|^2.
\end{aligned}
\tag{3.33}
$$

For the first term on the right-hand side of (3.33), by using the Cauchy-Schwarz inequality and the average inequality, we obtain

$$
(\boldsymbol{u}_h^{k+1}-\hat{\boldsymbol{u}}_h^*,\tilde{\boldsymbol{u}}_h^{k+1}-\hat{\boldsymbol{u}}_h^*)\le\frac{1}{2}\|\boldsymbol{u}_h^{k+1}-2\boldsymbol{u}_h^k+\boldsymbol{u}_h^{k-1}\|^2+\frac{1}{2}\|\tilde{\boldsymbol{u}}_h^{k+1}-2\boldsymbol{u}_h^k+\boldsymbol{u}_h^{k-1}\|^2.
\tag{3.34}
$$

For the second term on the right-hand side of (3.33), by using Lemma 3.4 and average inequality, we obtain

$$
\begin{aligned}
2\kappa\tau C(\tilde{\boldsymbol{u}}_h^{k+1}-\hat{\boldsymbol{u}}_h^*,\hat{\boldsymbol{m}}_h^k,\boldsymbol{m}_h^{k+1}) &\le 2C_e\kappa\tau\|\tilde{\boldsymbol{u}}_h^{k+1}-\hat{\boldsymbol{u}}_h^*\|_{L^2(\Omega)}\|\hat{\boldsymbol{m}}_h^k\times\nabla\times\boldsymbol{m}_h^{k+1}\|_{\mathcal{G}}\\
&\le\frac{1}{2}\|\tilde{\boldsymbol{u}}_h^{k+1}-2\boldsymbol{u}_h^k+\boldsymbol{u}_h^{k-1}\|^2+2C_e^2\kappa^2\tau^2\|\hat{\boldsymbol{m}}_h^k\times\nabla\times\boldsymbol{m}_h^{k+1}\|_{\mathcal{G}}^2.
\end{aligned}
\tag{3.35}
$$

For the third term on the right-hand side of (3.33), by using (3.28) and (3.6) and setting $\sigma_e\ge\tilde{C}_k^2$, we get

$$
\begin{aligned}
\frac{\tau}{\lambda\nu}\|S_h^{k+1}-S_h^k\|^2 &\le 2\lambda\nu\tau(\|\nabla_h\cdot\tilde{\boldsymbol{u}}_h^{k+1}\|^2+\|F_h([\![\tilde{\boldsymbol{u}}_h^{k+1}]\!])\|^2)\\
&\le 2\lambda\nu\tau(\|\nabla_h\tilde{\boldsymbol{u}}_h^{k+1}\|^2+\tilde{C}_k^2\sum_{e\in\mathcal{F}_h}h_e^{-1}\|[\![\tilde{\boldsymbol{u}}_h^{k+1}]\!]\|_{L^2(e)}^2)\\
&\le 2\lambda\nu\tau\|\tilde{\boldsymbol{u}}_h^{k+1}\|_{DG}^2.
\end{aligned}
\tag{3.36}
$$

By using (3.34)-(3.36) and without loss of generality, setting $\lambda=K_1$ and choosing the artificial parameter β such that $\kappa=\beta\tau/C_e^2$, the expression (3.33) becomes

$$
\begin{aligned}
&\frac{1}{2}\|\boldsymbol{u}_h^{k+1}\|^2+\frac{1}{2}\|2\boldsymbol{u}_h^{k+1}-\boldsymbol{u}_h^k\|^2+\frac{\kappa}{2}\|\boldsymbol{m}_h^{k+1}\|^2+\frac{\kappa}{2}\|2\boldsymbol{m}_h^{k+1}-\boldsymbol{m}_h^k\|^2\\
&+\frac{2\tau^2}{3}|||\psi_h^{k+1}|||_E^2+\frac{\tau}{\lambda\nu}\|S_h^{k+1}\|^2+\frac{\kappa}{2}\|\boldsymbol{m}_h^{k+1}-2\boldsymbol{m}_h^k+\boldsymbol{m}_h^{k-1}\|^2\\
&+2\kappa\nu_m\tau|||\boldsymbol{m}_h^{k+1}|||_D^2+2\kappa\nu_m\tau\|\boldsymbol{m}_h^{k+1}\|_C^2+\frac{2\tau^2}{9}|||z_h^{k+1}|||_E^2\\
&\le\frac{1}{2}\|\boldsymbol{u}_h^k\|^2+\frac{1}{2}\|2\boldsymbol{u}_h^k-\boldsymbol{u}_h^{k-1}\|^2+\frac{\kappa}{2}\|\boldsymbol{m}_h^k\|^2+\frac{\kappa}{2}\|2\boldsymbol{m}_h^k-\boldsymbol{m}_h^{k-1}\|^2+\frac{2\tau^2}{3}|||\psi_h^k|||_E^2+\frac{\tau}{\lambda\nu}\|S_h^k\|^2,
\end{aligned}
$$

which implies (3.17). The proof is complete. □

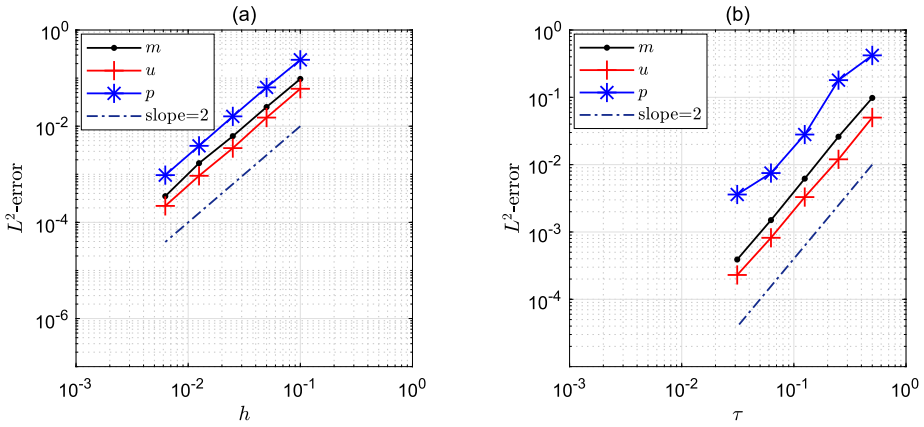

Fig. 4.1. The L^2 errors for the magnetic field $\boldsymbol{m}$, velocity field $\boldsymbol{u}$, and pressure p at time $t = 1$, where (a) convergence order in space, and (b) convergence order in time.

4. Numerical simulations

This section presents a series of numerical experiments aimed at assessing the effectiveness of the proposed scheme in accuracy and stability. Specifically, we employ the inf-sup stable P_2-P_1 element for the velocity field $\boldsymbol{u}$ and pressure p, and the P_2 element for the magnetic field $\boldsymbol{m}$.

4.1. Accuracy and stability tests

The first numerical example is to verify the convergence rates of the proposed scheme in time and space, where the domain is set as $\Omega = [0,1]\times[0,1]$. We choose the boundary conditions such that the exact solution satisfies

$$\begin{cases} \boldsymbol{m} = (-t^4 \sin(2\pi y)\cos(2\pi x), t^4 \sin(2\pi x)\cos(2\pi y)), \\ \boldsymbol{u} = (t^4 \sin^2(\pi x)\sin(2\pi y), -t^4 \sin(2\pi x)\sin^2(\pi y)), \\ p = t^4 \sin(2\pi x)\sin(2\pi y). \end{cases}$$

We set the model parameters as $\nu = \nu_m = \kappa = 1$ and $\lambda = 1$, and compute the numerical errors between the numerical solution and the exact solution at $t = 1$.

To confirm the convergence rates in space, we set the artificial parameter $\beta = 1$, fix the time step size $\tau = 0.01$, and choose decreasing spatial mesh sizes $h = 0.1/2^i, i = 0,1,2,3,4$. Fig. 4.1(a) displays the L^2-errors of the magnetic field $\boldsymbol{m}$, velocity field $\boldsymbol{u}$, and pressure p, demonstrating that the proposed scheme achieves second-order convergence in the spatial direction. To test the temporal convergence rates, we set $\beta = 0.1$ and fix the mesh size $h = 1/100$. Fig. 4.1(b) illustrates the convergence rates in time for all variables obtained by reducing temporal mesh sizes $\tau = 0.5/2^i, i = 0,1,2,3,4$. The results indicate that the magnetic field $\boldsymbol{m}$ and velocity field $\boldsymbol{u}$ achieve a convergence rate of second-order, while the time accuracy of pressure p is also nearly second-order.

We further verify the energy stability of the proposed scheme through another numerical test. We set the computational domain as $\Omega = [0,1]\times[0,1]$, the initial conditions for $\boldsymbol{m}, \boldsymbol{u}$ and p are given by:

$$\begin{cases} \boldsymbol{m}_0 = (\sin^2(\pi x)\sin(2\pi y), -\sin(2\pi x)\sin^2(\pi y)), \\ \boldsymbol{u}_0 = (-\sin(2\pi y)\cos(2\pi x), \sin(2\pi x)\cos(2\pi y)), \\ p_0 = \sin(2\pi x)\sin(2\pi y). \end{cases}$$

We consider the parameters $\nu = \nu_m = \kappa = 0.1$, $\lambda = 0.5$, and $\beta = \kappa/\tau$, and a fixed spatial mesh size of $h = 1/50$. We plot the energy evolution curves in Fig. 4.2, computed using different time steps $\tau = 0.5, 0.1, 0.05, 0.01$, up to the final time $T = 2.5$. These obtained energy curves indicate that the proposed scheme is unconditionally energy stable, as all energy curves decay monotonically for all tested time steps.

4.2. 2D Kelvin-Helmholtz instability

The K-H instability is a well-known hydrodynamic instability that arises when two fluid streams with different velocities flow parallel to each other, resulting in a velocity difference across the interface. In the context of MHD system, the K-H instability can occur when a sheared plasma flow is present in the presence of a magnetic field. The presence of a magnetic field can provide some stabilization to the flow, but the velocity shear across the interface can still induce instability in the flow. This instability can result in the generation of turbulence and mixing within the plasma, which can have significant consequences for astrophysical and geophysical phenomena, such as solar flares, accretion disks, and atmospheric dynamics, see [7,15,47].

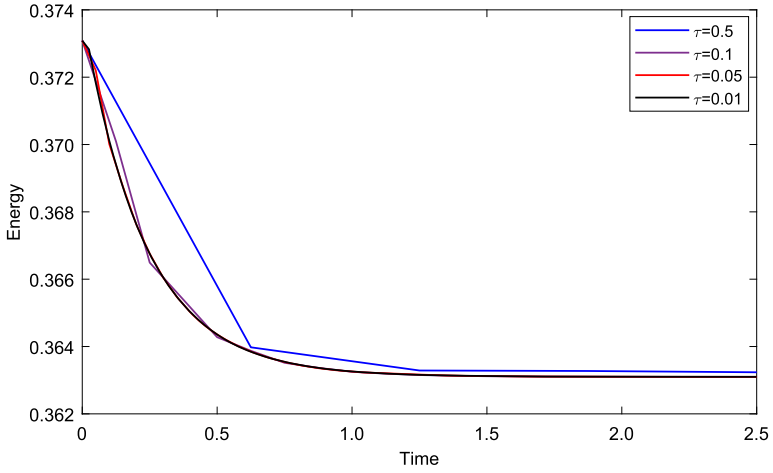

Fig. 4.2. Time evolution of the total energy functional $\mathbb{E}_{\text{tot}}^{h}$ computed using various time steps.

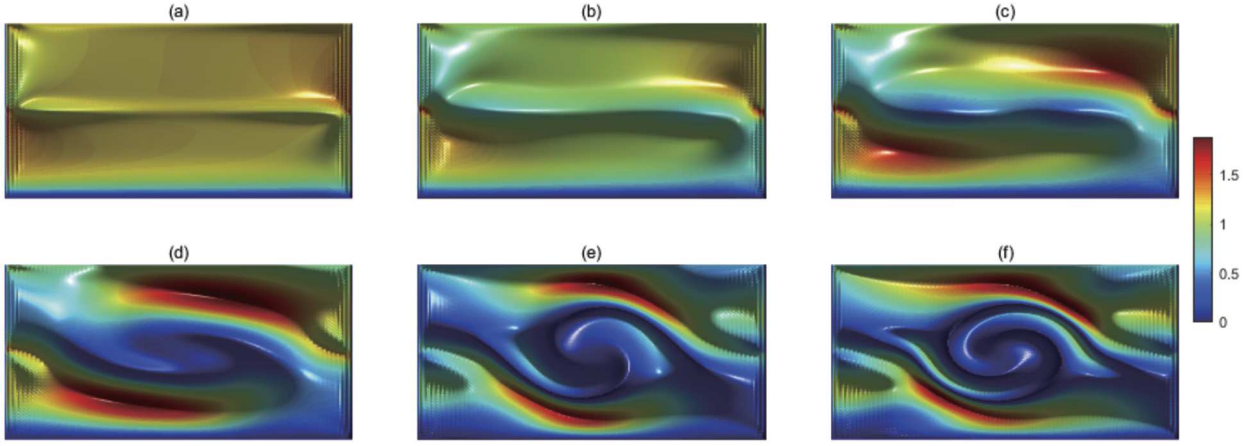

Fig. 4.3. Surface plots of $|\boldsymbol{m}|$ are taken at $t = 0.05,\ 0.1,\ 0.5,\ 0.8,\ 1.2,\ 1.5$ from (a) to (f).

In this example, we investigate the occurrence of K-H instability in a configuration of a single shear flow regime with a uniform magnetic field aligned with the flow direction. The computational domain is set as $\Omega = [0, 2] \times [0, 1]$, and the model parameter is set as $\nu = \nu_m = 0.01, \kappa = 0.2, \beta = 10, \lambda = 0.5, \tau = 0.01, h = 0.01$. The initial velocity field is $\boldsymbol{u}_0 = (1.5, 0)$ in the top half domain, and $\boldsymbol{u}_0 = (-1.5, 0)$ in the lower half domain, respectively. The initial magnetic field with shear is $\boldsymbol{m}_0 = (\tanh(y/\epsilon), 0)$ where $\epsilon = 0.07957747154595$. The magnetic field $\boldsymbol{m}$, velocity field $\boldsymbol{u}$, and pressure p all have periodic type boundary conditions on the left and right boundaries. The boundary conditions for $\boldsymbol{m}$ are set as $\boldsymbol{m} \times \boldsymbol{n} = \boldsymbol{m}_0 \times \boldsymbol{n}$ on the top and $\boldsymbol{m} \times \boldsymbol{n} = -\boldsymbol{m}_0 \times \boldsymbol{n}$ on the bottom, the second component of $\boldsymbol{u} = (u, v)$ on both the top and bottom boundaries is set as $v = 0$.

Figs. 4.3 and 4.4 show surface plots of the simulation results for the magnitude of the magnetic field $|\boldsymbol{m}|$ and velocity field $|\boldsymbol{u}|$ at times $t = 0.05, 0.1, 0.5, 0.8, 1.2, 1.5$, respectively. In Fig. 4.5, snapshots of the magnetic field $\boldsymbol{m}$ (Fig. 4.5(a1)-(c1)) and velocity field $\boldsymbol{u}$ (Fig. 4.5(a2)-(c2)) at $t = 0.05, 0.8, 1.5$ are displayed. Around time $t = 0.5$, vortexes start to form in the simulation, and by $t = 0.8$, the magnetic and velocity fields exhibit the characteristic structure of K-H instability with clearly visible vortex profiles. These images illustrate the interaction between the sheared velocity field and the magnetic field, producing a central vortex and bending the magnetic field due to the K-H instability.

4.3. 2D MHD rotor

The interaction between a magnetic field and a liquid metal like mercury can lead to a phenomenon known as the MHD effect. This intriguing phenomenon is observed when a liquid mercury rotator is exposed to a magnetic field, causing the mercury to form vortices or eddies that are perpendicular to the rotation axis and magnetic field lines. These fascinating patterns are created by the interaction between the magnetic field and the current induced by the rotating mercury and can be influenced by factors such as speed of rotation, the temperature of the mercury, and strength and direction of the magnetic field. Moreover, experiments involving the MHD rotor can provide valuable insights into the properties of liquid metals and the behavior of plasmas, which are ionized gases commonly studied in fusion research. In this study, we carry out numerical simulations of the MHD rotor as described in [23,33].

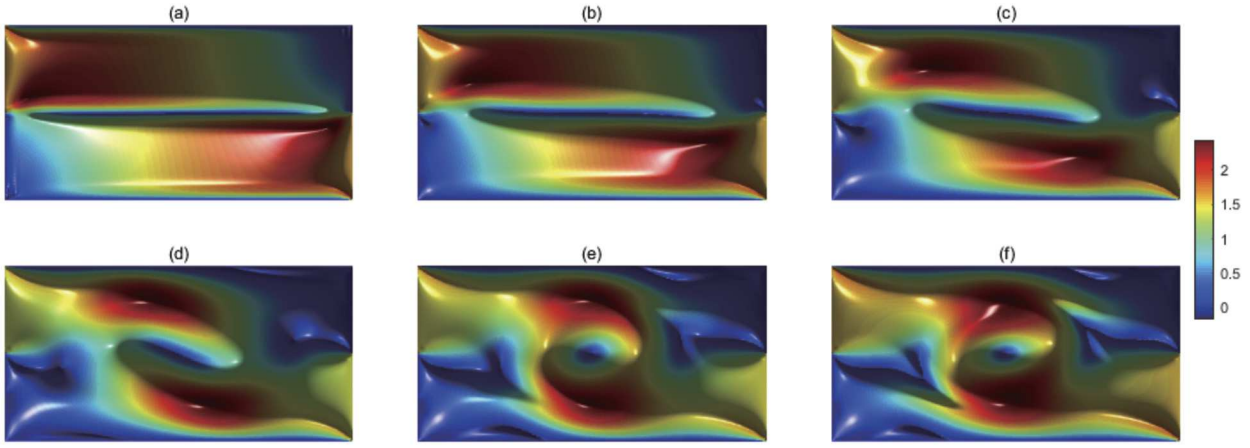

Fig. 4.4. Surface plots of $|\boldsymbol{u}|$ are taken at $t = 0.05$, 0.1, 0.5, 0.8, 1.2, 1.5 from (a) to (f).

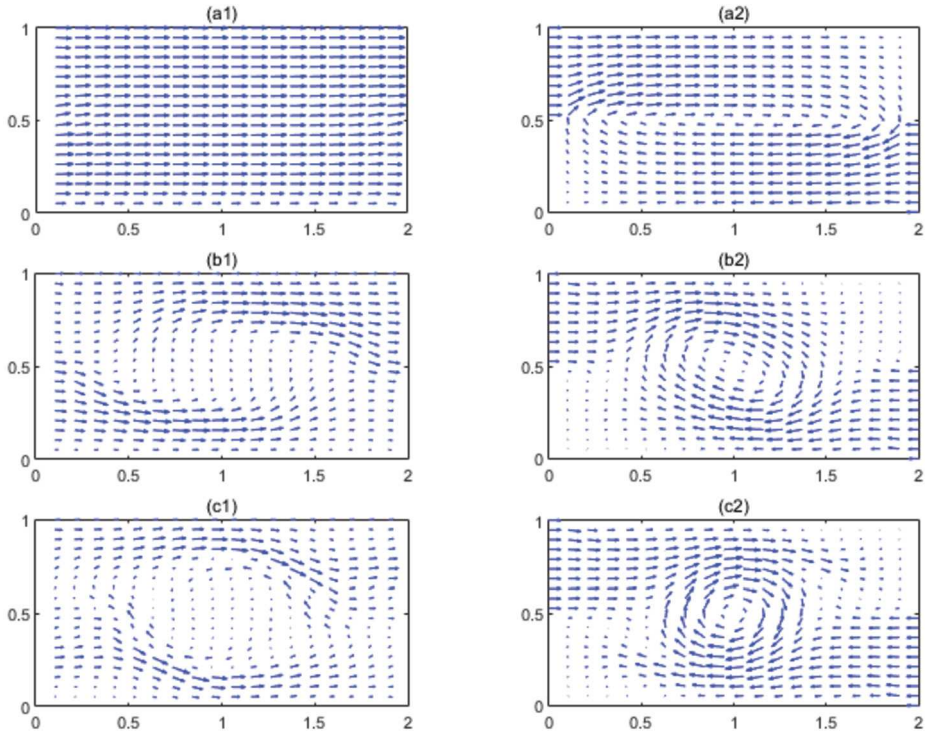

Fig. 4.5. Snapshots of the magnetic field $\boldsymbol{m}$ (left) and velocity field $\boldsymbol{u}$ (right) at $t = 0.05$, 0.8, and 1.5.

We set the computational domain as $\Omega = \{(x, y) : (x-0.5)^2 + (y-0.5)^2 = 1\}$ and the initial conditions as follows:

$$\boldsymbol{m}_0 = (\frac{5}{4\sqrt{\pi}}, 0),\ \boldsymbol{u}_0 = \phi(r)(5-10y, 10x-5),$$

where $r = \sqrt{(x-0.5)^2 + (y-0.5)^2}$ and

$$\phi(r) = \begin{cases} 1, \text{ if } r \le 0.1 \\ (23-200r)/3, \text{ if } 0.1 < r < 0.115, \\ 0, \text{ if } r \ge 0.115. \end{cases}$$

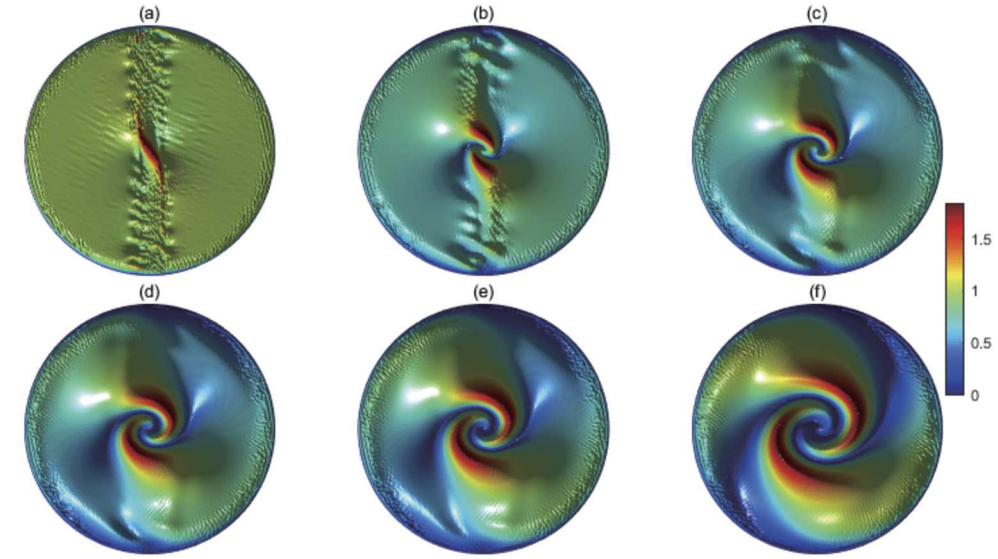

Fig. 4.6. Surface plot of the simulation result $|\boldsymbol{m}|$ at times $t = 0.03$, 0.1, 0.3, 0.5, 0.8, and 1.2 from (a) to (f).

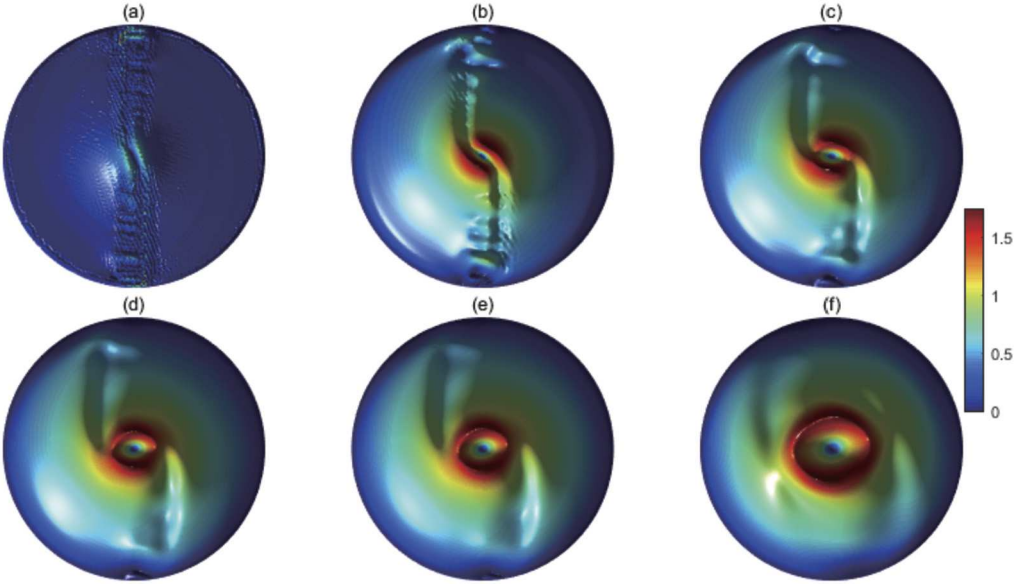

Fig. 4.7. Surface plot of the simulation result $|\boldsymbol{u}|$ at times $t = 0.03$, 0.1, 0.3, 0.5, 0.8, and 1.2 from (a) to (f).

The model parameters are set as $\nu = \nu_m = 0.01, \kappa = 0.2, \beta = 10, \lambda = 0.5, \tau = 0.01, h = 1/100$. The boundary conditions on the top and bottom boundaries are set as $\boldsymbol{m} \cdot \boldsymbol{n} = \boldsymbol{u} \cdot \boldsymbol{n} = 0$, while periodic type boundary conditions of $\boldsymbol{m}$ and $\boldsymbol{u}$ are used on the left and right boundaries.

In Fig. 4.6 and Fig. 4.7, surface plots of the magnetic field magnitude $|\boldsymbol{m}|$ and velocity field magnitude $|\boldsymbol{u}|$ are presented at selected times $t = 0.03$, 0.1, 0.3, 0.5, 0.8, and 1.2. Fig. 4.8 depicts the experimental setup of a magnetohydrodynamic rotor where liquid mercury is subjected to a magnetic field, alongside the corresponding magnetic and velocity fields obtained from our numerical simulations for comparison. The direction of the applied magnetic field in Fig. 4.8(b) is opposite to that in Fig. 4.8(a), enabling observation of the flow field in the exact opposite direction. This comparison highlights the sensitivity of the system to changes in the magnetic field direction, suggesting that our computational simulations are qualitatively consistent with the physical experiments.

4.4. 3D Taylor-Green vortex

The 3D Taylor-Green vortex is a flow field that serves as a popular benchmark problem for testing numerical simulations of MHD. It arises when a magnetic field is applied to a fluid, causing the formation of vortices that interact with the magnetic field. The resulting flow is characterized by strong vortices and complex interaction between the fluid and magnetic fields. As a widely used

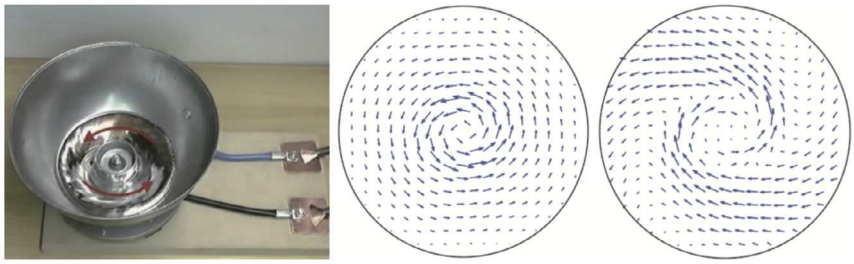

(a) Comparison of an experimental photograph of a liquid mercury rotator with the calculated velocity field $\boldsymbol{u}$ and magnetic field $\boldsymbol{m}$ at $t = 1.2$.

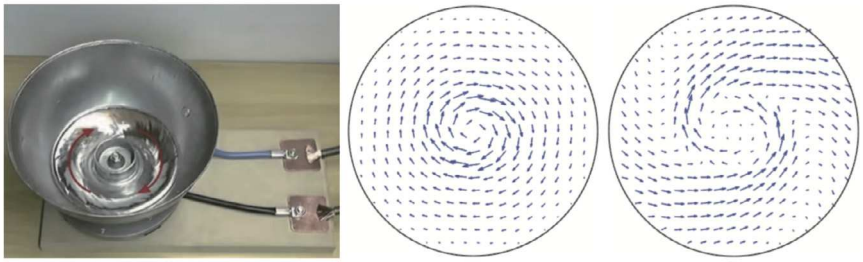

(b) Comparison of an experimental photograph of a liquid mercury rotator with the calculated velocity field $\boldsymbol{u}$ and magnetic field $\boldsymbol{m}$ at $t = 1.2$, after reversing the applied magnetic field.

Fig. 4.8. Comparison of an experimental photograph of a liquid mercury rotator (https://www.youtube.com/watch?v=bSIzyk5Mjko) with the computed velocity field $\boldsymbol{u}$ and magnetic field $\boldsymbol{m}$.

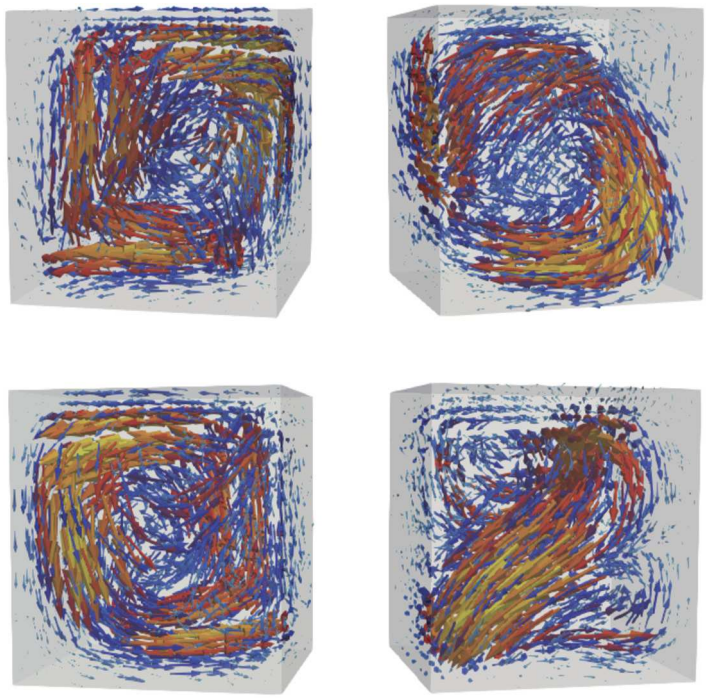

Fig. 4.9. Snapshots of the velocity field $\boldsymbol{u}$ at $t = 2.5$ with $\nu_m = 1$.

benchmark problem in MHD, the 3D Taylor-Green vortex is employed to assess the accuracy and effectiveness of MHD simulation methods.

In this example, we carry out the 3D MHD turbulence simulation with a Taylor-Green flow, see also in [16,37]. We set the computed domain as $\Omega = [0, 1] \times [0, 1] \times [0, 1]$ and the model parameters as $\nu = 1, \kappa = 1.0, \beta = 1, \lambda = 0.5, \tau = 0.1, h = 1/10$. The parameter

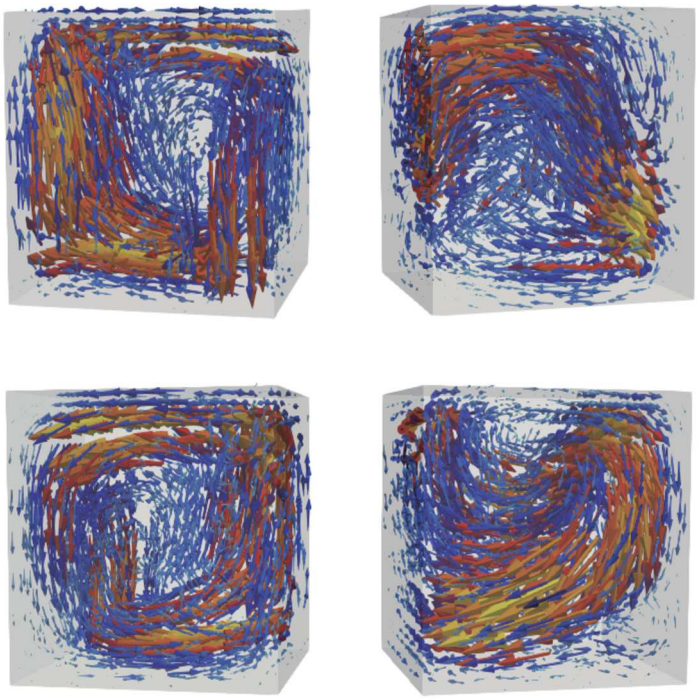

Fig. 4.10. Snapshots of the velocity field $\boldsymbol{u}$ at $t = 2.5$ with $\nu_m = 0.01$.

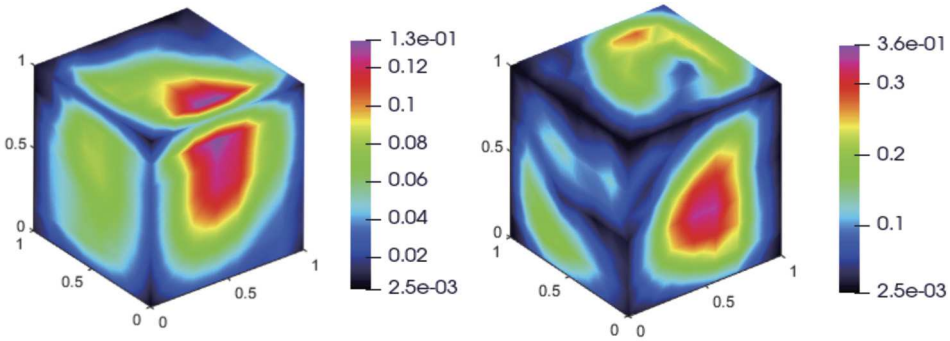

Fig. 4.11. Snapshots of the velocity field $|\boldsymbol{u}|$ at $t = 2.5$ with $\nu_m = 1$ and $\nu_m = 0.01$.

ν_m will be varied thereafter so that we can investigate the effects of the magnetic Reynolds number. The initial velocity field is the Taylor-Green vortex (see [16]), which is defined as

$$\boldsymbol{u}_0 = (\sin x \cos y \cos z, -\cos x \sin y \cos z, 0),$$

and the initial magnetic field is given by

$$\boldsymbol{m}_0 = (\cos x \sin y \sin z, \sin x \cos y \sin z, -2 \sin x \sin y \cos z).$$

The no-slip boundary conditions are imposed on the velocity field $\boldsymbol{u}$, and the magnetic field $\boldsymbol{m}$ satisfies the condition $\boldsymbol{m} \times \boldsymbol{n} = 0$ on the walls.

In Fig. 4.9-4.10, we show the computed simulation results of the velocity field $\boldsymbol{u}$ with two magnetic Reynolds numbers, $\nu_m = 1$ and 0.01, at a different angle, respectively. The magnitude of $|\boldsymbol{u}|$ at time $t = 2.5$ in these two cases is shown in Fig. 4.11. It can be seen that the flow is disordered with dominant warm vortices, which is typical of developed turbulence. Furthermore, the structure of the vortices is influenced by the magnetic Reynolds number.

5. Conclusion

This study proposes a novel approach to the problem by offering a second-order accurate, unconditionally energy-stable, and linear discontinuous Galerkin scheme for solving the nonlinearly coupled MHD system. The proposed scheme is achieved by intro-

ducing an additional stabilization term in the Maxwell equations, and by utilizing implicit-explicit treatments for dealing with the nonlinear and coupling terms, while a second-order pressure-correction scheme is used for solving the Navier-Stokes equations. The proposed numerical scheme requires solving only a few linear, fully decoupling equations at each time step. Unconditional energy stability in the discrete level is derived, and the unique solvability of the fully discrete scheme is strictly proved. Numerous numerical experiments, including the K-H instability, MHD rotator, and 3D Taylor-Green vortex, are conducted to evaluate the accuracy and stability of the proposed scheme. The numerical results demonstrate that the scheme performs robustly and accurately, achieving high levels of accuracy and stability across a variety of test cases.

CRediT authorship contribution statement

Guang-an Zou: Methodology, Implementation, Writing – Original draft preparation. **Bo Wang:** Conceptualization, Methodology, Implementation. **Xiaofeng Yang:** Methodology, Writing – Reviewing and Editing.

Declaration of competing interest

The authors declare that they have no known competing financial interests or personal relationships that could have appeared to influence the work reported in this paper.

Data availability

No data was used for the research described in the article.

Acknowledgements

The authors are grateful to the reviewers for the constructive comments and valuable suggestions which have improved the paper. G. Zou was partially supported by the Key Scientific Research Project of Colleges and Universities in Henan Province, China (23A110006). X. Yang was partially supported by NSF DMS-2012490 and DMS-2309731.

References

[1] J. Adler, T. Benson, E. Cyr, S. MacLachlan, R. Tuminaro, Monolithic multigrid methods for two-dimensional resistive magnetohydrodynamics, SIAM J. Sci. Comput. 38 (1) (2016) B1–B24.
[2] M. Akbas, S. Kaya, L. Rebholz, On the stability at all times of linearly extrapolated BDF2 timestepping for multiphysics incompressible flow problems, Numer. Methods Partial Differ. Equ. 33 (4) (2017) 999–1017.
[3] R. An, Y. Li, Error analysis of first-order projection method for time-dependent magnetohydrodynamics equations, Appl. Numer. Math. 112 (2017) 167–181.
[4] R. An, C. Zhang, Y. Li, Temporal convergence analysis of an energy preserving projection method for a coupled magnetohydrodynamics equations, J. Comput. Appl. Math. 386 (2021) 523–563.
[5] S. Badia, R. Codina, R. Planas, On an unconditionally convergent stabilized finite element approximation of resistive magnetohydrodynamics, J. Comput. Phys. 234 (2013) 399–416.
[6] S. Badia, R. Planas, J. Gutiérrez-Santacreu, Unconditionally stable operator splitting algorithms for the incompressible magnetohydrodynamics system discretized by a stabilized finite element formulation based on projections, Int. J. Numer. Methods Eng. 93 (3) (2013) 302–328.
[7] H. Baty, R. Keppens, P. Comte, The two-dimensional magnetohydrodynamic Kelvin-Helmholtz instability: compressibility and large-scale coalescence effects, Phys. Plasmas 10 (2003) 4661–4674.
[8] P. Chandrashekar, B. Nkonga, A. Bhole, A discontinuous Galerkin method for a two dimensional reduced resistive MHD model, Comput. Fluids 190 (2019) 178–191.
[9] Y. Cai, H. Choi, J. Shen, Error estimates for time discretizations of Cahn-Hilliard and Allen-Cahn phase-field models for two-phase incompressible flows, Numer. Math. 137 (2017) 417–449.
[10] Y. Cai, J. Shen, Error estimates for a fully discretized scheme to a Cahn-Hilliard phase-field model for two-phase incompressible flows, Math. Comput. 87 (2018) 2057–2090.
[11] H. Choi, J. Shen, Efficient splitting schemes for magneto-hydrodynamic equations, Sci. China Math. 59 (2016) 1495–1510.
[12] B. Cockburn, G. Kanschat, D. Schötzau, C. Schwab, Local discontinuous Galerkin methods for the Stokes system, SIAM J. Numer. Anal. 40 (1) (2002) 319–343.
[13] B. Cockburn, G. Karniadakis, C. Shu, The Development of Discontinuous Galerkin Methods, Springer, 2000.
[14] M. Costabel, M. Dauge, Weighted regularization of Maxwell equations in polyhedral domains, Numer. Math. 93 (2002) 239–277.
[15] E. Cyr, J. Shadid, R. Tuminaro, R. Pawlowski, L. Chacón, A new approximate block factorization preconditioner for two-dimensional incompressible (reduced) resistive MHD, SIAM J. Sci. Comput. 35 (2013) B701–B730.
[16] V. Dallas, A. Alexakis, Symmetry breaking of decaying magnetohydrodynamic Taylor-Green flows and consequences for universality, Phys. Rev. E 88 (6) (2013) 63017.
[17] D. Di Pietro, A. Ern, Discrete functional analysis tools for discontinuous Galerkin methods with application to the incompressible Navier-Stokes equations, Math. Comput. 79 (271) (2010) 1303–1330.
[18] A. Diegel, C. Wang, X. Wang, S. Wise, Convergence analysis and error estimates for a second order accurate finite element method for the Cahn-Hilliard-Navier-Stokes system, Numer. Math. 137 (3) (2017) 495–534.
[19] A. Fasoli, S. Brunner, W. Cooper, J. Graves, P. Ricci, O. Sauter, L. Villard, Computational challenges in magnetic-confinement fusion physics, Nat. Phys. 12 (2016) 411–423.
[20] X. Feng, Fully discrete finite element approximations of the Navier-Stokes-Cahn-Hilliard diffuse interface model for two-phase fluid flows, SIAM J. Numer. Anal. 44 (2006) 1049–1072.
[21] X. Feng, Y. He, C. Liu, Analysis of finite element approximations of a phase field model for two-phase fluids, Math. Comput. 76 (258) (2007) 539–572.
[22] C. Février, J. Laminie, P. Poullet, Ph. Angot, On the penalty-projection method for the Navier-Stokes equations with the MAC mesh, J. Comput. Appl. Math. 226 (2009) 228–245.

[23] E. Gawlik, F. Gay-Balmaz, A finite element method for MHD that preserves energy, cross-helicity, magnetic helicity, incompressibility, and $\mathrm{div}\, B = 0$, J. Comput. Phys. 450 (2022) 110847.
[24] J. Gerbeau, A stabilized finite element method for the incompressible magnetohydrodynamic equations, Numer. Math. 87 (2000) 83–111.
[25] J. Gerbeau, C. Bris, T. Leliévre, Mathematical Methods for the Magnetohydrodynamics of Liquid Metals. Numerical Mathematics and Scientific Computation, Oxford University Press, New York, 2006.
[26] V. Girault, B. Rivière, DG approximation of coupled Navier-Stokes and Darcy equations by Beaver-Joseph-Saffman interface condition, SIAM J. Numer. Anal. 47 (3) (2009) 2052–2089.
[27] V. Girault, B. Rivière, M. Wheeler, A splitting method using discontinuous Galerkin for the transient incompressible Navier-Stokes equations, ESAIM: M2AN 39 (6) (2005) 1115–1147.
[28] M. Grotea, A. Schneebelia, Interior penalty discontinuous Galerkin method for Maxwell's equations: optimal L^2-norm error estimates, IMA J. Numer. Anal. 28 (2008) 440–468.
[29] J. Guermond, J. Shen, On the error estimates for the rotational pressure-correction projection methods, Math. Comput. 73 (248) (2004) 1719–1737.
[30] J. Guermond, P. Minev, J. Shen, An overview of projection methods for incompressible flows, Comput. Methods Appl. Mech. Eng. 195 (2006) 6011–6045.
[31] M. Gunzburger, A. Meir, J. Peterson, On the existence, uniqueness, and finite element approximation of solutions of the equations of stationary, incompresible magnetohydrodynamics, Math. Comput. 56 (1991) 523–563.
[32] U. Hasler, A. Schneebeli, D. Schötzau, Mixed finite element approximation of incompressible MHD problems based on weighted regularization, Appl. Numer. Math. 51 (2004) 19–45.
[33] R. Hiptmair, C. Pagliantini, Splitting-based structure preserving discretizations for magnetohydrodynamics, SMAI J. Comput. Math. 4 (2018) 225–257.
[34] P. Houston, I. Perugia, A. Schneebeli, D. Schötzau, Interior penalty method for the indefinite time-harmonic Maxwell equations, Numer. Math. 100 (2005) 485–518.
[35] P. Houston, D. Schötzau, X. Wei, A mixed DG method for linearized incompressible magnetohydrodynamics, J. Sci. Comput. 40 (2009) 281–314.
[36] Y. Huang, J. Li, W. Yang, Interior penalty DG methods for Maxwell's equations in dispersive media, J. Comput. Phys. 230 (2011) 4559–4570.
[37] E. Lee, M. Brachet, A. Pouquet, P. Mininni, D. Rosenberg, Lack of universality in decaying magnetohydrodynamic turbulence, Phys. Rev. E 81 (2010) 016318.
[38] Y. Li, C. Zhai, Unconditionally optimal convergence analysis of second-order BDF Galerkin finite element scheme for a hybrid MHD system, Adv. Comput. Math. 46 (5) (2020) 75.
[39] F. Li, C. Shu, Locally divergence-free discontinuous Galerkin methods for MHD equations, J. Sci. Comput. 22 (2005) 413–442.
[40] X. Li, W. Wang, J. Shen, Stability and error analysis of IMEX SAV schemes for the magneto-hydrodynamic equations, SIAM J. Numer. Anal. 60 (3) (2022) 1026–1054.
[41] C. Liu, B. Rivière, A priori error analysis of a discontinuous Galerkin method for Cahn-Hilliard-Navier-Stokes equations, CSIAM Trans. Appl. Math. 1 (1) (2020) 104–141.
[42] R. Masri, C. Liu, B. Rivière, A discontinuous Galerkin pressure correction scheme for the incompressible Navier-Stokes equations: stability and convergence, Math. Comput. 91 (336) (2022) 1625–1654.
[43] A. Nacev, C. Beni, O. Bruno, B. Shapiro, The behaviors of ferro-magnetic Nano-particles in and around blood vessels under applied magnetic fields, J. Magn. Magn. Mater. 323 (6) (2011) 651–668.
[44] J. Pyo, Error estimates for the second order semi-discrete stabilized Gauge-Uzawa method for the Navier-Stokes equations, Int. J. Numer. Anal. Model. 10 (1) (2013) 24–41.
[45] W. Qiu, K. Shi, A mixed DG method and an HDG method for incompressible magnetohydrodynamics, IMA J. Numer. Anal. 40 (2019) 1356–1389.
[46] B. Rivière, Discontinuous Galerkin Methods for Solving Elliptic and Parabolic Equations: Theory and Implementation, Philadelphia, SIAM, 2008.
[47] D. Ryu, T. Jones, A. Frank, The magnetohydrodynamic Kelvin-Helmholtz instability: a three-dimensional study of nonlinear evolution, Astrophys. J. 545 (2000) 475–493.
[48] J. Shen, X. Yang, Energy stable schemes for Cahn-Hilliard phase-field model of two-phase incompressible flows, Chin. Ann. Math., Ser. B 31 (2010) 743–758.
[49] J. Shen, X. Yang, A phase-field model and its numerical approximation for two-phase incompressible flows with different densities and viscositites, SIAM J. Sci. Comput. 32 (2010) 1159–1179.
[50] C. Wang, J. Wang, Z. Xia, L. Xu, Optimal error estimates of a Crank-Nicolson finite element projection method for magnetohydrodynamic equations, ESAIM: M2AN 56 (3) (2022) 767–789.
[51] K. Wang, G. Zhang, Unconditionally energy stable, splitting schemes for magnetohydrodynamic equations, Int. J. Numer. Methods Fluids 93 (2021) 1396–1418.
[52] X. Wang, G. Zou, B. Wang, The stabilized penalty-projection finite element method for the Navier-Stokes-Cahn-Hilliard-Oono system, Appl. Numer. Math. 165 (2021) 376–413.
[53] T. Warburton, G. Karniadakis, A discontinuous Galerkin method for the viscous MHD equations, J. Comput. Phys. 152 (1999) 608–641.
[54] X. Yang, G. Zhang, X. He, Convergence analysis of an unconditionally energy stable projection scheme for magneto-hydrodynamic equations, Appl. Numer. Math. 136 (2019) 235–256.
[55] G. Zhang, Y. He, Decoupled schemes for unsteady MHD equations. I. Time discretization, Numer. Methods Partial Differ. Equ. 33 (3) (2017) 956–973.
[56] G. Zhang, X. He, X. Yang, A decoupled, linear and unconditionally energy stable scheme with finite element discretizations for magneto-hydrodynamic equations, J. Sci. Comput. 81 (2019) 1678–1711.
[57] G. Zhang, X. He, X. Yang, A fully decoupled linearized finite element method with second-order temporal accuracy and unconditional energy stability for incompressible MHD equations, J. Comput. Phys. 448 (2022) 110752.
[58] G. Zhang, M. Yang, Y. He, Block preconditioners for energy stable schemes of magnetohydrodynamics equations, Numer. Methods Partial Differ. Equ. 39 (2023) 501–522.
[59] G. Zhang, Y. Zhang, Y. He, Two-level coupled and decoupled parallel correction methods for stationary incompressible magnetohydrodynamics, J. Sci. Comput. 65 (2015) 920–939.
[60] Z. Zheng, G. Zou, B. Wang, W. Zhao, A fully-decoupled discontinuous Galerkin method for the nematic liquid crystal flows with SAV approach, J. Comput. Appl. Math. 429 (2023) 115207.
[61] G. Zou, B. Wang, X. Yang, A fully-decoupled discontinuous Galerkin approximation of the Cahn-Hilliard-Brinkman-Ohta-Kawasaki tumor growth model, ESAIM: M2AN 56 (2022) 2141–2180.
[62] G. Zou, Z. Li, X. Yang, Fully discrete discontinuous Galerkin numerical scheme with second-order temporal accuracy for the hydrodynamically coupled lipid vesicle model, J. Sci. Comput. 95 (2023) 5.